Tectonics

RESEARCH ARTICLE
10.1029/2020TC006348

Key Points:

- Syn-orogenic extrusion is proposed as a viable mechanism for the exhumation of HP-LT rock units of the Northern Apennines;
- The Acquadolce Subunit of the Eastern Elba nappe stack was exhumed by upward extrusion within an actively shortening orogenic wedge;
- Middle Miocene extension shaped the upper Northern Apennines orogenic wedge but did not contribute to the early exhumation of HP rocks.

Supporting Information:

Supporting Information may be found in the online version of this article.

Correspondence to:

G. Viola,
giulio.viola3@unibo.it

Citation:

Ryan, E., Papeschi, S., Viola, G., Musumeci, G., Mazzarini, F., Torgersen, E., et al. (2021). Syn-orogenic exhumation of high-P units by upward extrusion in an accretionary wedge: Insights from the Eastern Elba nappe stack (Northern Apennines, Italy). *Tectonics*, *40*, e2020TC006348. https://doi.org/10.1029/2020TC006348

Received 7 JUN 2020
Accepted 27 MAR 2021

Syn-Orogenic Exhumation of High-P Units by Upward Extrusion in an Accretionary Wedge: Insights From the Eastern Elba Nappe Stack (Northern Apennines, Italy)

E. Ryan[1], S. Papeschi[2], G. Viola[3], G. Musumeci[4,5], F. Mazzarini[5], E. Torgersen[1,6], B. E. Sørensen[1], and M. Ganerød[6]

[1]Department of Geoscience and Petroleum, Norwegian University of Science and Technology, Trondheim, Norway, [2]Kochi Institute for Core Sample Research, Institute for Extra-cutting-edge Science and Technology Avant-garde Research (X-star), JAMSTEC, Kanagawa, Japan, [3]Dipartimento di Scienze Biologiche, Geologiche ed Ambientali, Università degli Studi di Bologna, Bologna, Italy, [4]Dipartimento di Scienze della Terra, Università di Pisa, Pisa, Italy, [5]Istituto Nazionale di Geofisica e Vulcanologia, Pisa, Italy, [6]Geological Survey of Norway, Trondheim, Norway

Abstract The E-vergent Northern Apennines formed by Oligocene-Miocene convergence and westward subduction of Adria beneath Europe. Extension ensued in the Mid-Late Miocene reflecting lower plate roll-back and causing opening of the back-arc Northern Tyrrhenian Sea. Post-orogenic extension is commonly advocated as the main driver of the exhumation of the belt's inner domain high-pressure/low-temperature (HP-LT) rock units. The Acquadolce Subunit of the Eastern Elba nappe stack contains HP-LT rocks recording peak blueschist conditions of 1.5–1.8 GPa at 320°C–370°C loosely dated to the Oligocene-Early Miocene. It is sandwiched by two Late Miocene, out-of-sequence top-to-the E thrusts between Jurassic LP serpentinites on top and HT–LP contact metamorphosed marbles at its base. We document widespread W-verging ductile asymmetries within the Acquadolce Subunit, which correspond to top-to-the W extensional shearing for the nappe stack current orientation. This allowed for early syn-orogenic exhumation from blueschist- to greenschist-facies conditions, wherein coeval W-directed extension at the top of the exhuming units acted synchronously with E-directed thrusting at their base causing exhumation by extrusion in an overall contractional setting. The basal, E-vergent thrusting is, however, challenging to document as the wedge has since been reworked by Late Miocene, E-verging compressive tectonics, contact metamorphism, and later extension, obliterating much of the evidence supporting exhumation by extrusion during the early stages of wedge build-up. Syn-orogenic exhumation by extrusion from deep structural levels within the orogenic wedge is a viable mechanism to account for other exhumed HP-LT units in the inner part of the belt.

1. Introduction

Exhumed high-pressure/low-temperature (HP-LT) rocks and terranes occur worldwide in both active and fossil collision zones reflecting complex subduction zone processes (Ernst, 1970, 1972; Hamilton, 1969; Malusà et al., 2015; Miyashiro, 1972; Okay et al., 1989; O'Brien, 2019; Tsujimori & Ernst, 2014). HP-LT blueschists and eclogites are typically found in units derived from the subducted oceanic crust (e.g., Agard et al., 2009). Continental margins, however, may also be pulled into the subduction channel by the downgoing oceanic slab, and undergo high- to ultra-high-pressure (UHP) metamorphism (e.g., Chopin, 1984, 2003; Coleman & Wang, 1995; Smith, 1984; Sobolev & Shatsy, 1990). Many authors argue that the introduction of low-density continental material into subduction zones interrupts the subduction process after *c.* 10 million years from the onset of underthrusting, eventually leading to continental collision (Chopin, 2003; Duchêne et al., 1997; Ernst, 2001). The exhumation of HP-LT continental units generally begins during convergence, shortly after the metamorphic peak (Avigad et al., 1997; Reddy et al., 1999; Ring et al., 1999; Ring, Will, et al., 2007), at very fast rates, comparable to those of plate tectonics (Ernst et al., 1997; Glodny et al., 2005; Rubatto & Hermann, 2001). Whereas the P-T paths and rates of exhumation are relatively straightforward to constrain and thus reasonably well-known, uncertainty remains regarding the exhumation mechanisms, particularly at early stages of the process due to the low preservation potential of early structures. Several, often contrasting exhumation models have, therefore, been proposed (see reviews by Platt [1993], Maruyama et al. [1996], Kurz and Froitzheim [2002], and Warren [2013]), such as upward transport of HP-LT

rocks in diapirs (England & Holland, 1979), return flow of viscous material in subduction channels or accretionary wedges (Cloos, 1982; Cowan & Silling, 1978; Gerya et al., 2002), collapse of overthickened thrust wedges during underplating (Davis et al., 1983; Platt, 1986), low-angle normal faulting and exhumation in metamorphic core complexes (Lister & Davis, 1989; Lister et al., 1986; Whitney et al., 2013), and extrusion along coeval and oppositely verging extensional and thrust faults (Hacker et al., 1995; Ring, Will, et al., 2007). Some models require erosion and removal of overburden above the exhuming material, for example, the channel flow model (Beaumont et al., 2001; Chemenda et al., 1995; Godin et al., 2006).

Circum-Mediterranean belts, where HP-LT rocks were exhumed to the surface during the Africa-Eurasia collision, are a good study area to investigate this process. Multidisciplinary studies in the Alps and in the Aegean, for instance, have documented the occurrence of HP-LT units sandwiched between lower grade rocks (e.g., Avigad et al., 1997; Escher & Beaumont, 1997; Kurz & Froitzheim, 2002; Michard et al., 1993; Reddy et al., 1999; Ring & Layer, 2003; Thomson et al., 1999; Wheeler et al., 2001), bounded by coeval and oppositely verging shear zones (Glodny et al., 2005; Ring, Will, et al., 2007, Ring, Glodny, et al., 2007; Ring & Glodny, 2010). Unfortunately, alternating compressive and extensional phases affected many circum-Mediterranean belts during the Cenozoic (Bonini et al., 2014; Jolivet & Brun, 2010; Malinverno & Ryan, 1986; Rosenbaum et al., 2002; Rosenbaum & Lister, 2004; Viola et al., 2018). These deformation phases partially to fully overprinted the evidence of early exhumation in the rock record and the models that have been proposed to explain local exhumation rely on the complex interplay of syn-orogenic extrusion and post-orogenic extension, often without conclusive direct constraints (Avigad et al., 1997; Behr & Platt, 2012; Jolivet et al., 1998, 2003; Ring et al., 2010; Rossetti et al., 2002; Searle & Lamont, 2020; van Hinsbergen et al., 2005).

Unraveling the exhumation history of HP-LT rocks is indeed a complex task that requires a complete range of structural, microstructural, and petrographic data, with geochemical and geochronological constraints. Unfortunately, mostly due to scarce exposures and/or subsequent obliterating tectonic histories, it is rarely possible to derive all these constraints, no matter how detailed the research effort. To explain the presence of HP-LT rocks at the surface, it is necessary to elaborate conceptual models, at times based on only partial and incomplete geological records.

The Northern Apennines of Italy, where exhumed HP-LT continental units have been reported from many areas over the past three decades (e.g., Brogi & Giorgetti, 2012; Bianco et al., 2015; Giorgetti et al., 1998; Jolivet, 1998; Rossetti et al., 1999, 2001; Theye et al., 1997), are one such case. No universally accepted unifying model exists to account for all details of their structural and kinematic framework and, in turn, for the tectonic mechanisms responsible for the exhumation of the exposed HP-LT units. This is mostly due to the lack of robust constraints on the early exhumation stages, which are only scantly documented in the rock record (Carmignani & Kligfield, 1990; Jolivet et al., 1998; Molli et al., 2018; Rossetti et al., 2002).

In this study, we contribute further to the understanding of this fundamental geodynamic issue by documenting widespread, W-verging structures in the E-verging Northern Apennines on the Island of Elba. We interpret these structures as effective potential drivers of the syn-orogenic exhumation of blueschist-facies continental rocks, which is key to understanding the spatial and temporal evolution of the Apennines. By means of field, structural, and microstructural data, we document, to the best of the possibilities offered by the available exposure, multiscalar top-to-the W deformation that we interpret as linked to exhumation of the HP rocks in the area. New $^{40}Ar/^{39}Ar$ dating, integrated with existing geochronological data, help constrain a minimum age of the peak blueschist-facies metamorphism to the early Miocene (19–21 Ma). We interpret the available data set as suggesting a process of syn-orogenic extrusion in the subduction channel, active during the early continental collision in the Northern Apennines, thus, predating the post-orogenic extension of the Northern Tyrrhenian Sea, which is classically interpreted as being the main, if not the only, driver of the documented fast exhumation up to shallow crustal levels.

2. Geological Outline

2.1. The Northern Apennines

The Northern Apennines (Figures 1a and 1b) are an active E-verging orogenic belt that resulted from the Cretaceous-Eocene subduction of the Alpine Tethys Ocean and the subsequent collision of the Adria microcontinent with the European continental margin (Boccaletti et al., 1971; Conti et al., 2020; Vai &

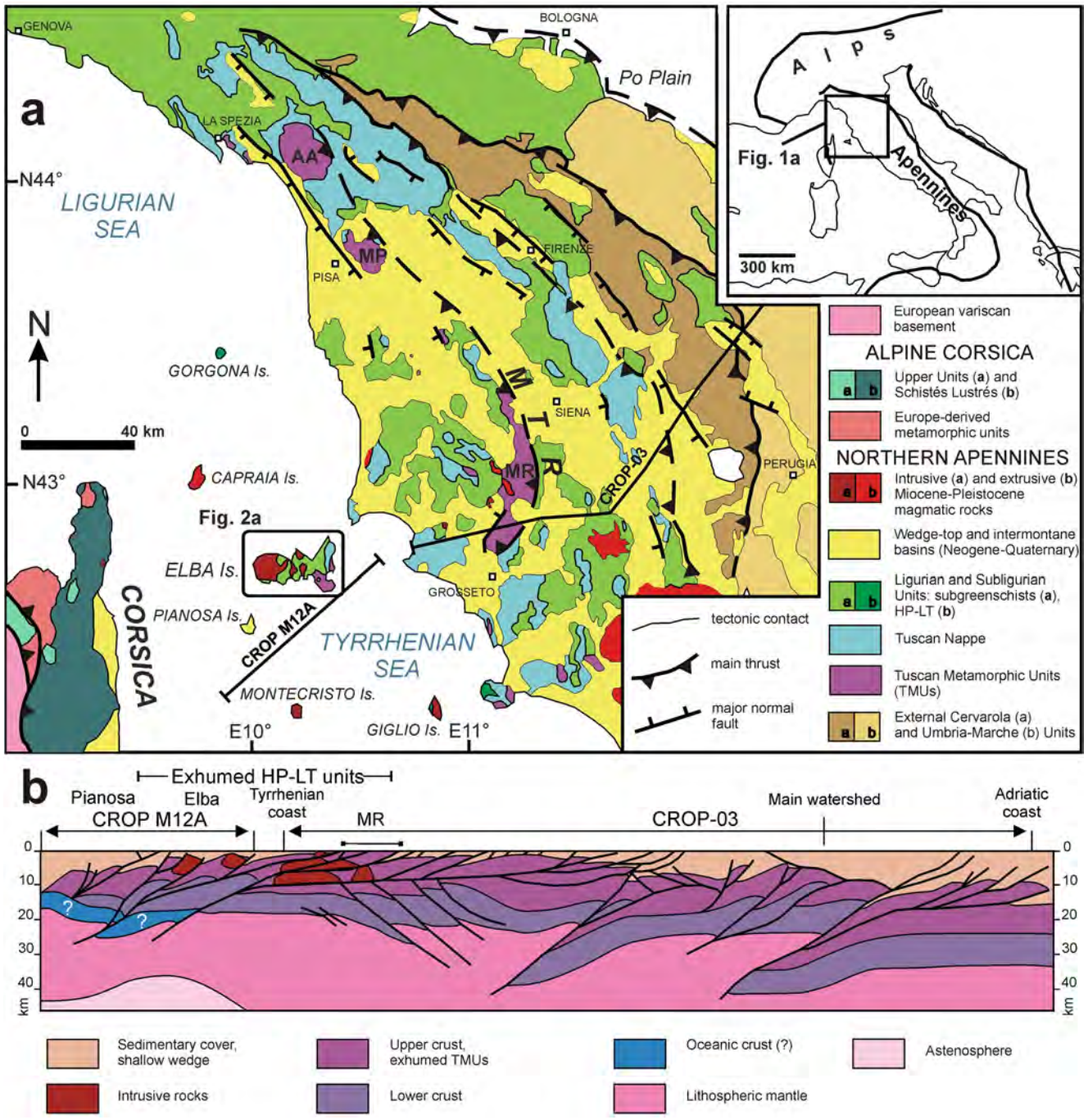

Figure 1. Regional geological setting of the Northern Apennines: (a) Tectonic sketch map of the Northern Apennines-Alpine Corsica orogenic system (modified after Bonini et al. [2014]) and traces of the CROP M12A and CROP-03 seismic profiles; (b) Interpreted profile along the CROP M12A and part of the CROP-03 seismic lines through the Northern Apennines (simplified after Finetti et al. [2001] and Bonini et al. [2014]). AA, Alpi Apuane; MP, Monti Pisani; MR, Monticiano-Roccastrada; MTR, Mid-Tuscan Ridge.

Martini, 2001). According to several authors, the Alpine Tethys Ocean closed due to an earlier E-dipping Late Cretaceous-Eocene subduction that culminated with the SW-verging "Alpine" orogeny in Corsica (Figure 1a). The following evolution was characterized by a regional E–NE-ward tectonic vergence, due either to a flip or an along-strike change of the earlier subduction polarity (e.g., Marroni et al., 2017; Molli & Malavieille, 2011; Vignaroli et al., 2008). After the onset of continental collision in the Oligocene, the Northern Apennines orogenic wedge widened and propagated toward the east-northeast, while extension, basin

development, and magmatism are believed to have occurred as part of a back-arc evolution in the hinterland of the belt, causing the opening of the Tyrrhenian Sea (Elter et al., 1975; Malinverno & Ryan, 1986; Serri et al., 1993). Back-arc spreading was continuous in the Southern Tyrrhenian Sea from the early Miocene to present (Malinverno & Ryan, 1986). In the Northern Tyrrhenian Sea, back-arc extension is also generally considered continuous since the early Miocene, accompanied by a coeval migration of the thrust front toward the Adriatic sea (Faccenna et al., 2001; Jolivet et al., 1998; Keller & Coward, 1996). In the Corsica Basin, syn-rift sequences suturing the relationships between Alpine Corsica and the Northern Apennines are dated to the Langhian-Messinian (Mauffret et al., 1999; Moeller et al., 2013). Extension in the hinterland of the Apennines east of the Corsica basin (including Elba) is believed to have commenced in the middle/late-Miocene and has been linked to exhumation of the deep orogenic roots (e.g., Carmignani et al., 1994; Carmignani & Kligfield, 1990; Daniel & Jolivet, 1995; Jolivet et al., 1998; Keller & Coward, 1996). In this conceptual framework, some authors have argued that exhumation was in part syn-orogenic and associated with cold exhumation paths and compressional structures predating back-arc extension in the region (e.g., Jolivet et al., 1998; Rossetti et al., 2002, 1999; Storti, 1995; Vignaroli et al., 2009). More recently, however, several studies have shown that extension in the Northern Apennines hinterland has been episodically interrupted by compressive pulses in the Late Miocene (e.g., Bonini et al., 2014; Bonini & Sani, 2002; Musumeci et al., 2008; Musumeci et al., 2015; Viola et al., 2018). At present, the Northern Apennines are characterized by active shortening at the easternmost front of the belt (Po Plain and Adriatic domains) coexisting with extension in the Northern Tyrrhenian Sea and internal sectors (Figure 1a; Boccaletti et al., 2011; Faccenna et al., 2014; Pauselli et al., 2006).

The main thrusts and tectonic lineaments of the belt strike NW–SE to N–S and invariably verge to the east (Figure 1a). In Figure 1b, we show one of the proposed interpretations of the deep lithospheric architecture of the Northern Apennines, adapted from the interpretation of CROP profiles by Finetti et al. (2001) and Bonini et al. (2014). This CROP profile shows that major reflectors (i.e. tectonic contacts) in the Northern Apennines are predominantly W-dipping and interpreted as regional-scale thrusts, as shown in Figure 1b. This model contrasts, however, with other interpretations of the CROP profiles, which tend to stress the presence of E-dipping low-angle normal fault systems (e.g., Pauselli et al., 2006). We consider the interpretation by Finetti et al. (2001) and Bonini et al. (2014) to be more in line with the actual geology of the Northern Tyrrhenian Sea as also depicted by other recent, high-resolution seismic profiles showing W-dipping reflectors, symmetric rifting, and no evidence of widespread, crustal-scale E-dipping low-angle normal faults (e.g., Moeller et al., 2013).

The Northern Apennines nappe stack consists of units derived from the oceanic and ocean–continent transition domains (Ligurian and Subligurian Units), thrust onto Adria-derived units (Tuscan Units; Figure 1a; Boccaletti et al., 1971; Elter, 1975). The Ligurian Units are generally unaffected by Alpine metamorphism, and HP-LT parageneses have been documented therein only in the belt hinterland on the Island of Gorgona (Figure 1a; P-T = 1.3–1.6 GPa at 300–350°C; 25.6 ± 0.3 Ma; Brunet et al., 2000; Jolivet et al., 1998; Rossetti et al., 2001), on the Island of Giglio (Figure 1a; P-T = 0.7–0.8 GPa at 300°C–350°C; Rossetti et al., 1999) and in the Monte Argentario area (Figure 1a; P-T ≥ 0.7 GPa at ∼340°C; Theye et al., 1997). Adria-derived units comprise (1) the subgreenschist-facies Tuscan Nappe (Carosi et al., 2003; Cerrina Feroni et al., 1983; Montomoli et al., 2001), which remained at upper structural levels and never experienced significant metamorphism, and (2) the Tuscan Metamorphic Units (TMUs; Figure 1a), which instead experienced up to blueschist-facies subduction-related metamorphism (Franceschelli et al., 2004; Jolivet et al., 1998). At a regional scale, the TMUs crop out in correspondence of culminations of the continental basement (Figure 1b). P-T estimates in the TMUs are in the 0.4–1.8 GPa and 300°C–500°C range (Brogi & Giorgetti, 2012; Giorgetti et al., 1998; Jolivet et al., 1998; Lo Pò & Braga, 2014; Molli et al., 2000; Papeschi et al., 2020; Vignaroli et al., 2009). Overall, the highest documented pressures in the TMU rock record are from the hinterland, from Monte Argentario (Figure 1a; P-T = 0.8–1.0 GPa at 350–420°C; Theye et al., 1997), the Island of Giglio (Figure 1a; P-T = 1.2–1.4 GPa at 310–350°C; Rossetti et al., 1999), and the Island of Elba (Figure 1a; P-T = 1.5–1.8 GPa at 320–370°C; Bianco et al., 2015, 2019; Papeschi et al., 2020).

As mentioned, exhumation of the TMUs was interpreted both as post-orogenic in a scenario of metamorphic core complex exhumation (Carmignani & Kligfield, 1990; Carmignani et al., 1994) and as resulting from a combination of syn- and post-orogenic extension (Jolivet et al., 1998; Molli et al., 2018; Rossetti

et al., 2002). Some authors have stressed the importance of thrusting during the early stages of exhumation leading to inverted tectonic gradients, as in the Alpi Apuane or on the Island of Giglio, where upper greenschist- and blueschist-facies rocks are thrust on top of lower greenschist-facies units (Carosi et al., 2004; Molli et al., 2000; Rossetti et al., 1999; Storti, 1995). Daniel and Jolivet (1995) and Jolivet et al. (1998) proposed low-angle normal faults as key structures for the exhumation of metamorphic units and emplacement of late Miocene plutons within the orogenic wedge. However, most of these structures have only been recognized within the shallowest parts of the wedge, presumably implying only limited throws (in the order of a few km; e.g., Musumeci et al., 2015) along moderately to steeply dipping normal faults, and interpreted either as syn- (Clemenzi et al., 2014; Massa et al., 2017) or post-orogenic extensional structures (Clemenzi et al., 2015; Collettini & Holdsworth, 2004).

2.2. The Island of Elba

Zooming into the geological framework of the Island of Elba reveals a stack of W-dipping and E/NE-verging thrust nappes intruded by Late Miocene plutonic rocks and cut by high- and low-angle normal faults (Figures 2a and 2b; Bortolotti et al., 2001; Collettini & Holdsworth, 2004; Keller & Coward, 1996; Massa et al., 2017; Pertusati et al., 1993). The nappe edifice is defined by thrust sheets stacked along N-S striking, top-to-the E/NE thrusts and is folded by E/NE-verging folds with N-S to NNE-SSW trending axes. E-W trending lineations are the main linear fabric of the stack, consistent with the overall E-vergence of the belt (Figures 2a and 2b; Keller & Coward, 1996; Massa et al., 2017). The nappe stack can be subdivided internally into an Upper and a Lower Complex (Musumeci & Vaselli, 2012), separated by the out-of-sequence Capo Norsi-Monte Arco Thrust (CN–MAT by Viola et al. [2018]), which is marked by a slice of tectonized serpentinite (Serpentinite Unit in Figure 2a) sandwiched between continental units (Figure 2a).

The Upper Complex, in the hanging wall of the Serpentinite Unit, is composed of a sequence of nonmetamorphic to anchizone-facies Ligurian and Tuscan Units, intruded by Late Miocene plutonic rocks of the Monte Capanne Pluton and the Central Elba Laccolith Complex in the west, and the Porto Azzurro Pluton in the east (Figure 2a; Barboni et al., 2015; Bouillin, 1983; Dini et al., 2002). Regional metamorphism in the Upper Complex is only locally observed in the lower greenschist-facies Rio Marina Unit (Figure 2a; Elter & Pandeli, 2001; Franceschelli et al., 1986).

The Lower Complex consists of the metamorphic Ortano and Calamita Units (Figure 2a). The Calamita Unit hosts the Porto Azzurro monzogranite (5.9 ± 0.2 Ma, $^{40}Ar/^{39}Ar$ biotite age, Maineri et al., 2003; 6.33 ± 0.07 Ma, $^{40}Ar/^{39}Ar$ biotite age, Musumeci et al., 2015), which is mostly below sea level. The intrusion of the Porto Azzurro monzogranite (Figures 2a and 2b) caused low-pressure/high-temperature (LP-HT) metamorphism, dated to between 6.76 ± 0.08 Ma ($^{40}Ar/^{39}Ar$ phlogopite age) and 6.23 ± 0.06 Ma ($^{40}Ar/^{39}Ar$ muscovite age; Musumeci et al., 2011, 2015). LP–HT metamorphism reached peak temperatures of 600–700°C in the Calamita Unit and 450–600°C in the Ortano Unit at $P < 0.2$ GPa (Duranti et al., 1992; Musumeci & Vaselli, 2012; Papeschi et al., 2019), almost completely obliterating pre-existing metamorphic parageneses. Only the Acquadolce Subunit, in the northern part of the Ortano Unit, still preserves regional glaucophane- and lawsonite-bearing HP-LT assemblages that escaped contact metamorphism (see below; Bianco et al., 2015, 2019; Papeschi et al., 2020).

According to Keller and Coward (1996), Pertusati et al. (1993), and Massa et al. (2017), the main collisional event took place in the Oligocene–Early Middle Miocene. During this period of time, the nappes were stacked, and the metamorphic units reached their peak conditions (e.g., ~19–20 Ma; Bianco et al., 2019; Deino et al., 1992) before being exhumed (Massa et al., 2017; Papeschi et al., 2020).

The Middle-Late Miocene was marked by the emplacement of large volumes of magma (Dini et al., 2002; Rocchi et al., 2010) up to shallow crustal levels in the nappe stack ($P < 0.2$ GPa; Duranti et al., 1992; Rossetti et al., 2007). Magma emplacement is generally interpreted as coeval with extensional tectonics, due to either gravitational collapse during intrusion (Daniel & Jolivet, 1995; Pertusati et al., 1993; Trevisan, 1950; Westerman et al., 2004) or regional crustal extension connected to the opening of the Northern Tyrrhenian Sea (Keller et al., 1994; Keller & Coward, 1996; Jolivet et al., 1998). Evidence in favor of this phase of extension includes high- and low-angle fault zones that crosscut the nappe pile. For instance, the Zuccale Fault (Figures 2a and 2b) is a subhorizontal fault zone with an eastward displacement of *c*. 6 km that has

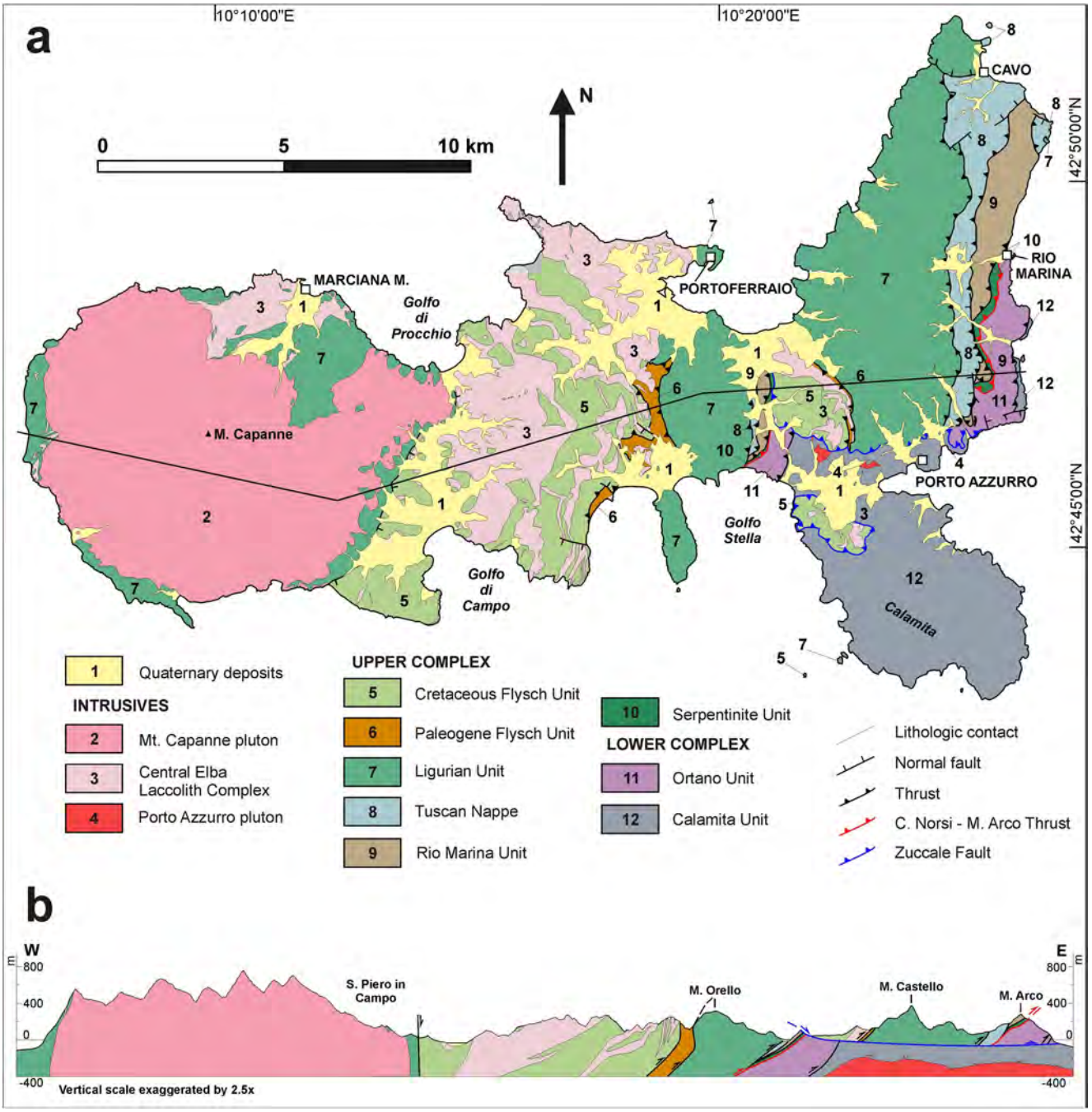

Figure 2. Geological setting of the Island of Elba: (a) Simplified structural-geological map of Elba (modified after Massa et al. [2017]). The frame denotes the study area. (b) Cross-section (roughly oriented E–W) across the island. Note that the vertical scale is exaggerated by 2.5×.

been almost invariably interpreted as a low-angle normal fault, accommodating significant post-orogenic extension and exhumation of the Porto Azzurro Pluton and the metamorphic Calamita Unit (Collettini & Holdsworth, 2004).

More recently, however, the extensional models have been questioned on Elba by the recognition of Late Miocene compressional structures shown to be coeval with magmatism and the associated LP–HT metamorphism. Mazzarini et al. (2011), Musumeci and Vaselli (2012), and Papeschi et al. (2017, 2018), for example, documented E-verging folds and top-to-the E shear zones with thrust kinematics that accompanied the development of the contact aureole of the Porto Azzurro Pluton. The CN-MAT itself was recognized as

an out-of-sequence thrust that superimposes the nonmetamorphic Upper Complex over amphibolite-facies hornfelses of the Lower Complex (Massa et al., 2017; Musumeci & Vaselli, 2012; Viola et al., 2018). Consequently, the interpretation of the Zuccale Fault as an extensional fault has been questioned in favor of its interpretation as a flat segment of a thrust (Musumeci et al., 2015; Viola et al., 2018). K/Ar dating of authigenic illite on the CN–MAT, the Zuccale Fault, and similar thrusts in the Lower Complex showed that a phase of thrusting was active until the early Pliocene between 6.14 ± 0.64 Ma and 4.90 ± 0.27 Ma (Viola et al., 2018) and that the last recorded phase of extension of the nappe stack started in the Pliocene and was accommodated by high-angle normal faults (Mazzarini et al., 2019; Musumeci et al., 2015).

3. Materials and Methods

To propose a self-consistent model capable of incorporating the geological evidence presented below, our study has implemented a multidisciplinary approach combining field work and structural analysis, petrography, microstructures, fabric analysis by Electron Back-Scattered Diffraction (EBSD), and $^{40}Ar/^{39}Ar$ thermochronology. We conducted detailed structural-geologic mapping over the ~2 km^2 area shown in Figures 3 and 4, selecting representative structural stations on well-exposed coastal outcrops of the Acquadolce Subunit. Thin sections cut parallel to the stretching lineation and shear direction (i.e., L_p lineation) and perpendicular to the regional and mylonitic foliation (S_p/S_m) were prepared from the main lithologies of the Acquadolce Subunit. Sample details are available in Table S1. Our EBSD analysis focused on calc-mylonitic material, as it best preserves the W-directed mylonitic shearing and kinematic indicators related to the deformation of the Acquadolce Subunit.

For the $^{40}Ar/^{39}Ar$ analysis, we selected a white mica-bearing sample (ELB5) from the Rio Marina outcrop (Area A in Figure 4). We chose this area because (1) it is located far away from the contact-metamorphosed rocks to the south and was less affected by thermal metamorphism, (2) the chemistry of the dated white mica is well known from companion samples from the same outcrop that was investigated by Papeschi et al. (2020), and (3) independent white mica $^{40}Ar/^{39}Ar$ dating was performed in the same area by Deino et al. (1992) and on glaucophane by Bianco et al. (2019). We also chose this specific sample because the white mica was relatively coarse-grained compared to other samples.

The analytical details of the EBSD analysis and $^{40}Ar/^{39}Ar$ dating are available in dedicated Appendixes A and B.

4. The Acquadolce Subunit of the Lower Complex

The Ortano Unit dips uniformly to the W and is composed, from bottom to top, of (1) a Middle Ordovician basement made of metarhyolites and metavolcanoclastics (Ortano Porphyroid Fm.), (2) a sequence of Jurassic metacarbonates (Ortano Marble Fm.), and (3) an overlying schistose complex, which we refer to as the Acquadolce Subunit (Figure 3; Duranti et al., 1992; Massa et al., 2017; Musumeci et al., 2011; Papeschi et al., 2020).

The Acquadolce Subunit is structurally bounded at its base by the Felciaio Shear Zone (FSZ; Musumeci & Vaselli, 2012) and at its top by the CN–MAT (Viola et al., 2018). The FSZ and CN–MAT are Late Miocene E-verging thrusts that accommodated shortening during and shortly after the emplacement of the Porto Azzurro Pluton at shallow crustal levels (Figure 3). These thrusts sandwiched the Acquadolce Subunit between serpentinites at its top and the diopside-bearing LP–HT Ortano Marble at its base (Figure 3). The contact-metamorphic overprint of the Porto Azzurro Pluton is spatially confined to the southernmost part of the Acquadolce Subunit (mostly south of Mt. Fico–Il Porticciolo; Figure 3). This thermal overprint is defined by distinctive cordierite and/or andalusite (Papeschi et al., 2020) statically overgrowing the lower grade schistose complex.

Lithologically, the Acquadolce Subunit comprises a sequence of light brown white mica + chlorite ± biotite schist with layers of quartz + K-feldspar + plagioclase-bearing metapsammite, metamarl, and graphitic schist (Acquadolce Schist). U-Pb dating of detrital zircon yielded a 31.6 ± 0.5 Ma maximum deposition age for the Acquadolce Schist in the Ortano Valley (Figure 3; Jacobs et al., 2018). The Acquadolce Schist also contains discontinuous layers and lenses of gray/white to green marble, calcschist, and cherty marble,

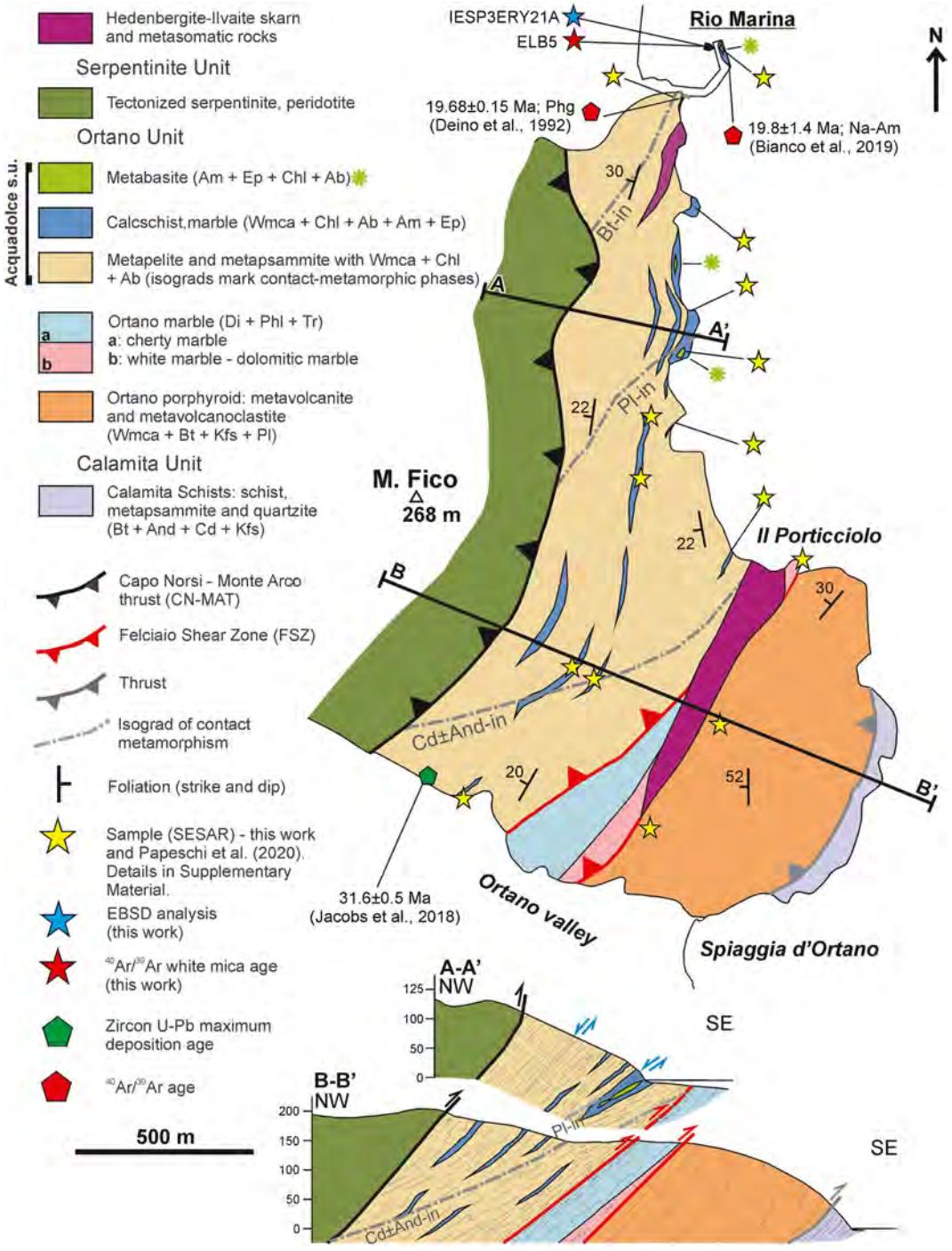

Figure 3. Geological sketch map of the Ortano Unit, north of the Ortano Valley, showing the position of samples (stars) and the isograds of contact metamorphism. Sample names are reported in the supporting information. Pentagons mark the location of the samples dated by Deino et al. (1992), Bianco et al. (2019), and Jacobs et al. (2018). For clarity, skarn bodies are not shown in the cross-sections. Mineral abbreviations after Siivola and Schmid (2007).

ranging from a few centimeters up to 15–20 m thick (Figure 3), which are loosely dated to the Mesozoic based on lithostratigraphic correlations (Duranti et al., 1992; Massa et al., 2017; Papeschi et al., 2020). These metacarbonates locally host 0.1–2.0 m thick lenses of green metabasite and metavolcanoclastic rock (detailed in Figure 3). The metabasite contains porphyroclasts of omphacitic clinopyroxene, associated with Na- and Ca-amphibole (glaucophane-crossite to actinolite), chlorite, epidote, titanite, phengite, and

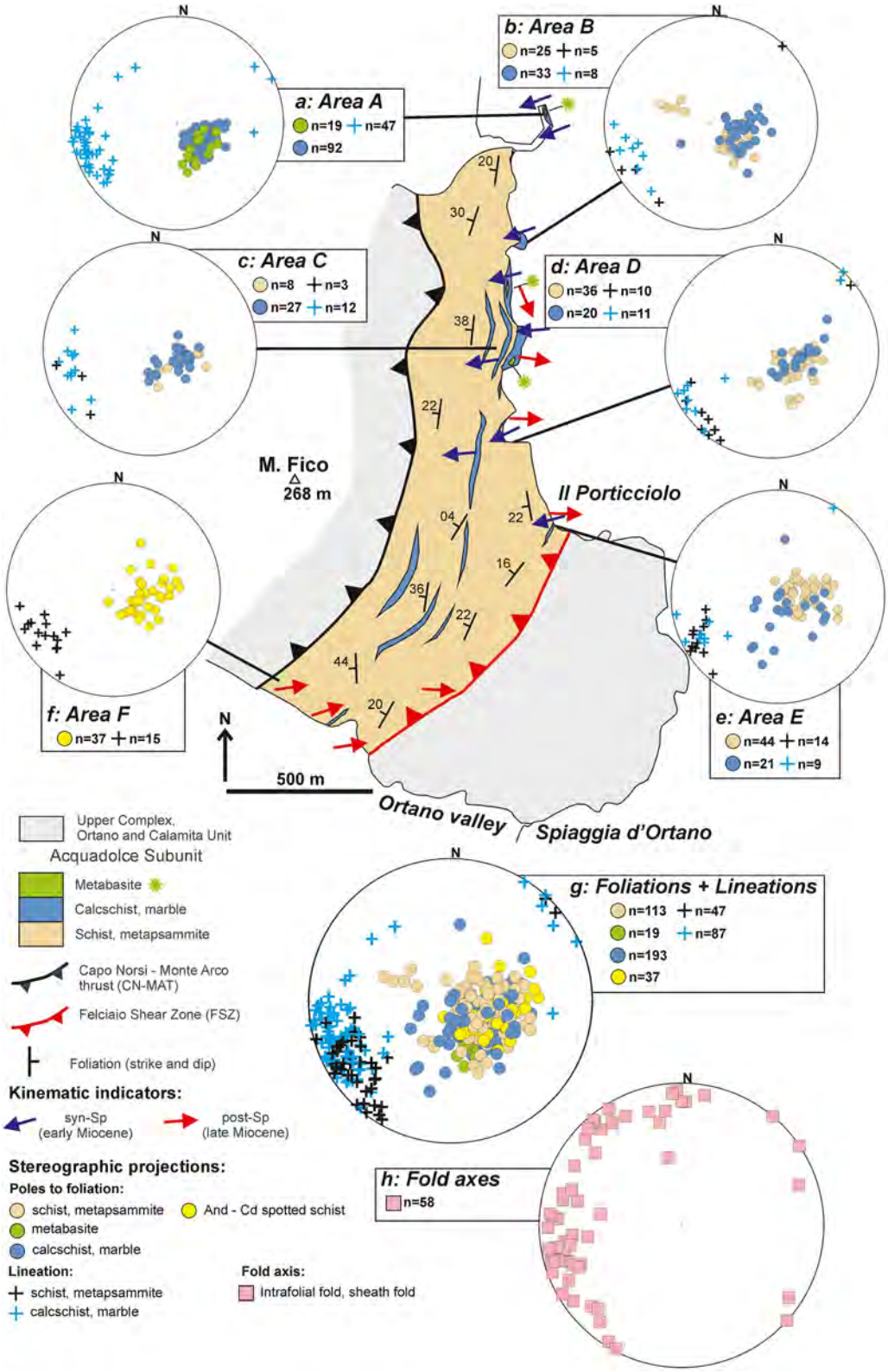

Figure 4. Structural map of the Acquadolce Subunit, highlighting the distribution of the main structural elements: (a–f) Foliation and lineation orientation in different subareas; (g) Cumulative orientation plot of structural elements; (h) Intrafolial fold axes. Stereographic projections are equal area, lower hemisphere projections. See text for details.

pseudomorphosed lawsonite (Bianco et al., 2015, 2019; Papeschi et al., 2020). Millimetric layers of chlorite-rich, Na-amphibole-bearing metabasic material are also present in the hosting calcschist. Papeschi et al. (2020) estimated peak P-T conditions of 1.5–1.8 GPa at 320–370°C for these rocks, while ^{40}Ar-^{39}Ar dating of phengite and glaucophane yielded ages of 19.68 ± 0.15 Ma (Deino et al., 1992) and 19.8 ± 1.4 Ma (Bianco et al., 2019).

5. Structural Framework of the Acquadolce Subunit

The principal foliation (S_p) and internal lithological contacts in the Acquadolce Subunit strike NNE–SSW and dip between 10° and 50° to the W/SW (Figure 4), with only very limited along-strike variations causing local northward and southward dips (e.g., Figures 4c–4e). In the metasediments of the Acquadolce Subunit, the S_p is defined by the metamorphic layering and the preferred orientation of greenschist- and blueschist-facies mineral grains (white mica, chlorite, quartz, calcite, albite, and Na-amphibole). Mineral lineations (L_p) on the foliation planes are defined by oriented aggregates and grains of quartz, calcite, mica, albite, Na-amphibole that trend from ENE-WSW to NE-SW with a general plunge between 10° and 40° (Figure 4) to the SW and only locally to the NE (e.g., Figures 4a, 4b, 4d, and 4e). Metabasite lenses, hosted in metacarbonates, are weakly foliated and contain strongly retrogressed lawsonite + Na-amphibole + omphacite surrounded by chlorite + epidote + Ca-amphibole + titanite.

The northern part of the study area, north of the B-B′ cross-section trace in Figure 3, contains well-preserved blueschist- and greenschist-facies parageneses where the LP-HT contact metamorphic overprint is weak to absent. North of the Mt. Fico-Il Porticciolo alignment (Figure 3), top-to-the W deformation is common and well-preserved (Figure 4) despite later, overprinting top-to-the E shear zones (red arrows in Figure 4). To the south in the Ortano Valley, the S_p strikes c. N-S, dips to the west (Figure 4f) and is defined by the syn-kinematic growth of LP-HT andalusite- and cordierite-bearing contact metamorphic parageneses of the Late Miocene Porto Azzurro Pluton. Top-to-the E shear zones (e.g., the FSZ; Musumeci & Vaselli, 2012) and E-verging mesoscale folds, coeval with the Late Miocene LP-HT metamorphism, are the dominant structures in this area (Figures 3 and 4) and obliterate the older structural record.

5.1. Top-To-The W Deformation in the Acquadolce Subunit

To clarify the role of the mapped W-verging structures within the Acquadolce Subunit, we describe the mesoscopic structural framework of the Acquadolce Subunit and its microstructural characteristics in more detail below.

5.2. Mesostructures

The Acquadolce Subunit is a generally highly strained unit that preserves hitherto ignored, yet significant, top-to-the W deformation associated with penetrative, generally N-S striking and W-dipping fabrics (Figures 4 and 5). Higher strain domains occur therein as centimetric to metric, W/SW-dipping mylonitic structures, which are particularly well-developed and preserved in the metacarbonatic lithologies (marble and calcschist; Figures 5a–5c). Metapelitic lithologies, characterized by lower competence compared to the metacarbonates, preserve well-foliated structures with local, recumbent W-verging, noncylindrical isoclinal folds in metapsammitic and metacarbonatic interlayers (supporting information). Competent metabasite lenses within the metacarbonates form boudins and pinch-and-swell structures and sometimes exhibit fractured necks infilled by calcite + quartz + dolomite ± chlorite ± white mica ± epidote ± titanite veins (Figure 5c). Asymmetric metabasite boudins display W-vergent asymmetries and are themselves segmented along W–SW-dipping, top-to-W shear planes (Figure 6a).

Within the metacarbonatic lithologies, a gradual and continuous transition from intensely foliated and fine-grained mylonite (with a mylonitic foliation that we refer to as S_m) to relatively less foliated and coarser calcschist and marble is common (Figure 5b). We interpret the S_m as the high-strain equivalent of the S_p, as both foliations are parallel and defined by the preferred orientation of the same mineral assemblage, namely calcite, quartz, white mica, chlorite, biotite, albite, and Na-amphibole. Lineations throughout the

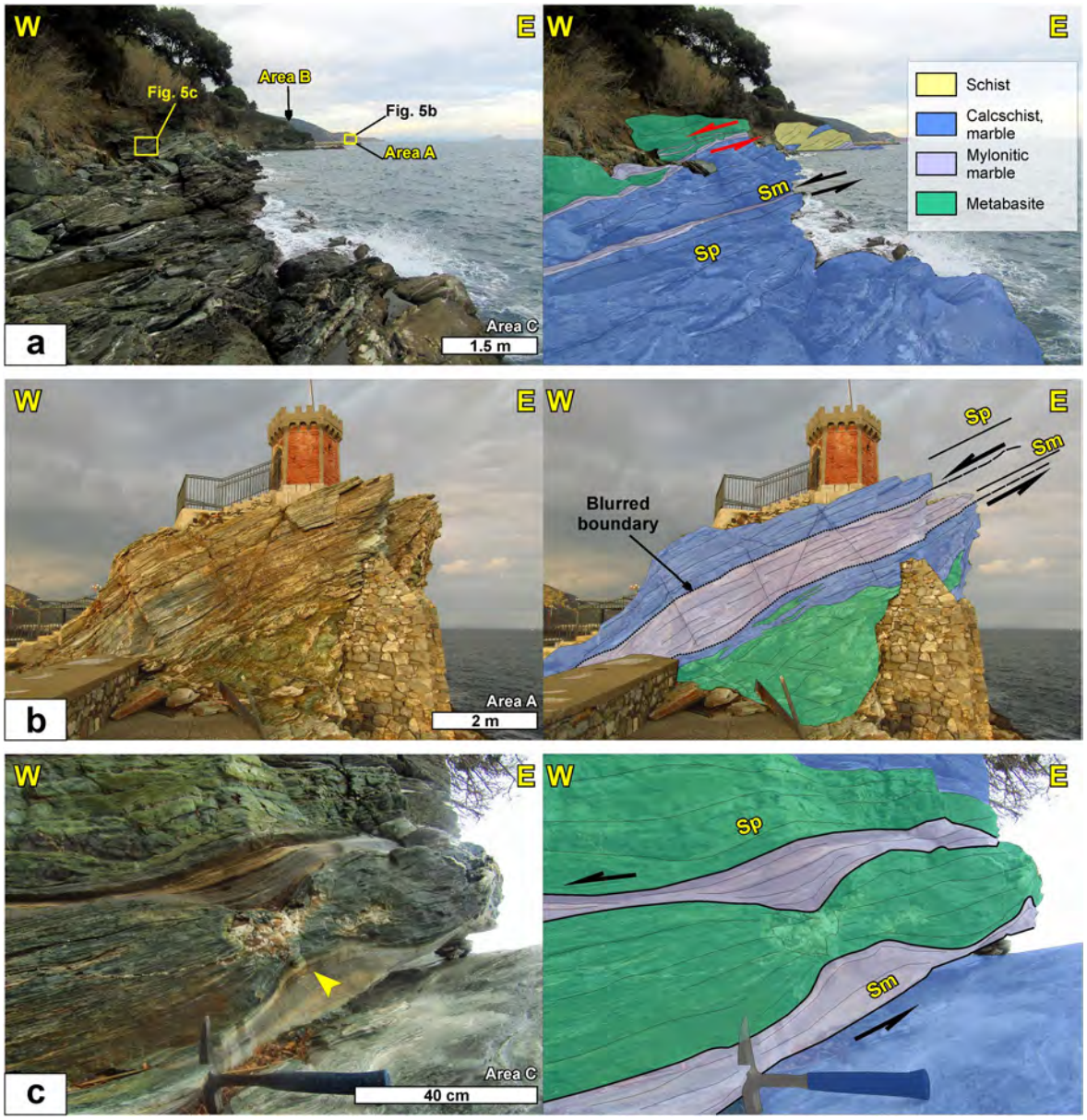

Figure 5. Mesoscale top-to-the W shear zones documented in (a–c) Area C and (b) Area A. *Note*. How shear zones are parallel to the main foliation. (c) Detail of a penetratively foliated mylonitic calcschist surrounding a boudinaged metabasite layer (pinch-and-swell structure). See text for details. S_m, mylonitic foliation; S_p, main foliation.

Acquadolce Subunit are invariably defined by the same mineral phases and monotonously trend from E-W to SW-NE.

The S_m in the mylonitic calcschist is defined by tightly spaced, sub-millimetric, subparallel to anastomosing layers of chlorite + Na-amphibole and carbonate minerals (Figure 6b). Foliation boudinage localizes in quartz and mica-rich layers that form neck structures filled by coarse-grained calcite (yellow arrow in Figure 6b). In places (e.g., area A—Rio Marina lighthouse, Figures 4 and 5b), the well-foliated mylonite contains centimetric to decimetric, highly transposed tight-to-isoclinal SW to NW-verging asymmetric folds with W-dipping axial planes, thickened hinges, and stretched limbs (Figure 6c). These folds exhibit strongly noncylindrical to sheath-like geometry and closed, elliptical fold surfaces (eye structures) are visible on N-S sections (Figure 6d), perpendicular to the E-W to SW-NE trending lineation. Fold axes are sub-horizontal, plunge gently (0°–10°) to the NNW-SW, and trend from N-S to E-W (Figure 4h).

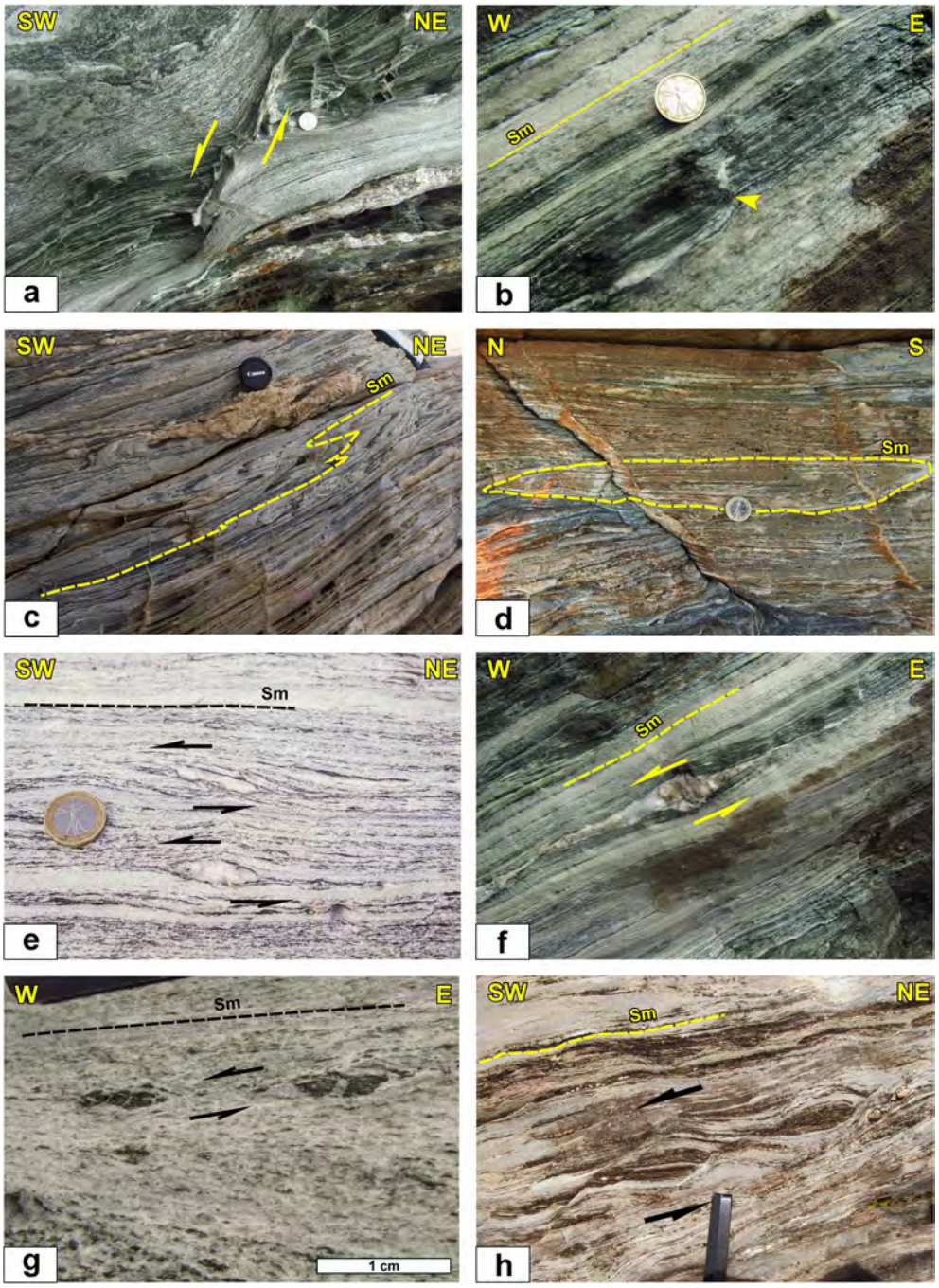

Figure 6. Mesoscale structures and kinematic indicators: (a) Asymmetric boudinage of a foliated metabasite layer in mylonitic calcschist, separated by top-to-the W shear fractures. (b) Foliation boudinage of a chlorite-rich layer in mylonitic calcschist with gaps (yellow arrow) filled by calcite. (c) W-verging mesoscale folds in mylonitic marble and calcschist. (d) N–S oriented section across a sheath fold, showing closed elliptical surfaces. (e) Mylonitic calcschist containing top-to-the W imbricated objects like small-scale duplexes (above) and sigmoidal structures (below), developed around coarse-grained calcite objects. (f) Sigmoidal aggregate of quartz and calcite, indicating top-to-the W sense of shear. (g) Top-to-the W C′ shear bands in mylonitic marble, developed around boudinaged metapelitic layers. (h) W-verging S-C′ structures localized around boudinaged layers of metachert in mylonitic marble. S_m, mylonitic foliation.

Table 1
Chart of blastesis/deformation relationships for phases in the calcschists of the Acquadolce Subunit

Metamorphic stage	Blueschists		Greenschists
Deformation phase	Pre-S_m	Syn-S_m	Post-S_m
Lawsonite*	■■■		
Na-amphibole	■■■	■■	
White mica	■■■	■■■	
Chlorite	■■■	■■■	
Epidote		■■■	■■■
Albite		■■■	■■■
Quartz	■■■	■■■	■■
Calcite	■■■	■■■	■■
Titanite		■■■	■■■
Rutile	■■■	■■	
Ilmenite		■■■	■■
Graphite	■■■	■■■	■■

*Denotes phases that are preserved only as pseudomorphs.

Top-to-the W kinematics in mylonite zones are reliably constrained by asymmetric, cm-scale intrafolial features including imbricated duplex-like stacks (Figure 6e), sigmoidal quartzitic, and carbonatic clasts (Figures 6e and 6f), and asymmetric mm-sized albite grains (see Section 6.2 below). C′-type shear bands (following Berthé et al., 1979) developed at low to very low angles to the S_m and deform the mylonitic metacarbonates with displacements ranging from a few millimeters to some centimeters, as measured on displaced layers of metabasite, metachert, and metapsammite (Figures 6g and 6h).

5.3. Microstructures

To clarify the temporal relationships between blastesis and deformation in the Acquadolce Subunit, we propose a conceptual chart depicting relative mineral growth stages with respect to S_m development (Table 1).

This indicative chart is based on numerous consistent microstructural observations from the present work and mineral chemistry data by Papeschi et al. (2020). Metamorphic parageneses of the investigated samples are given in Table S1.

At the microscopic scale, the mylonitic metacarbonates consist largely of a network of stretched and dynamically recrystallized calcite domains surrounding albite porphyroblasts and are interlayered with thin white mica + chlorite + Na-amphibole-bearing layers (Figure 7a). Calcite-rich domains range in thickness from a few millimeters to some centimeters and in places contain oriented, subparallel grains of white mica, chlorite, and Na-amphibole, as well as lobate quartz and albite grains. The microstructure of calcite consists of larger relic grains (0.1–1 mm in size), mantled by fine-grained calcite and crosscut by top-to-the W shear bands defined by fine-grained (10–50 μm) dynamically recrystallized calcite grains (Figure 7b). Relic calcite grains show ameboid to lobate boundaries with recrystallized bulges (10–50 μm in size), intracrystalline undulose extinction, and bent mechanical e-twins (type III of Ferrill et al., 2004). In the most strained samples, relic calcite grains are strongly elongated parallel to the S_m (e.g., Figures 7a and 7b). In others, they display a shape preferred orientation (SPO), defining an oblique foliation with respect to the S_m that is invariably consistent with a top-to-the W sense of shear (Figures 7c and 7d).

About 10–200 μm thick phyllosilicate-rich layers are commonly interlayered with the calcite-rich domains. They consist of fine-grained chlorite and white mica, associated with albite, epidote, quartz, Na-amphibole, retrogressed lawsonite, titanite, and accessory allanite, apatite, rutile, zircon, and tourmaline (in modal order). The presence of ilmenite and graphite is only restricted to a few samples (Table S1). Na-amphibole is locally replaced by aggregates of albite, white mica, chlorite, and biotite, whereas lawsonite is pseudomorphosed as clinozoisite–Fe-epidote aggregates and occurs mostly as inclusions in albite (e.g., Figure 9d; Bianco et al., 2019; Papeschi et al., 2020). White mica, chlorite, and Na-amphibole represent the main foliation-defining phases in the phyllosilicate-rich layers. As shown by Papeschi et al. (2020) and Bianco et al. (2015, 2019), white mica is invariably high in Si (Si p.f.u. = 3.3–3.6, based on 11 oxygens; Figure 11) and represents an HP

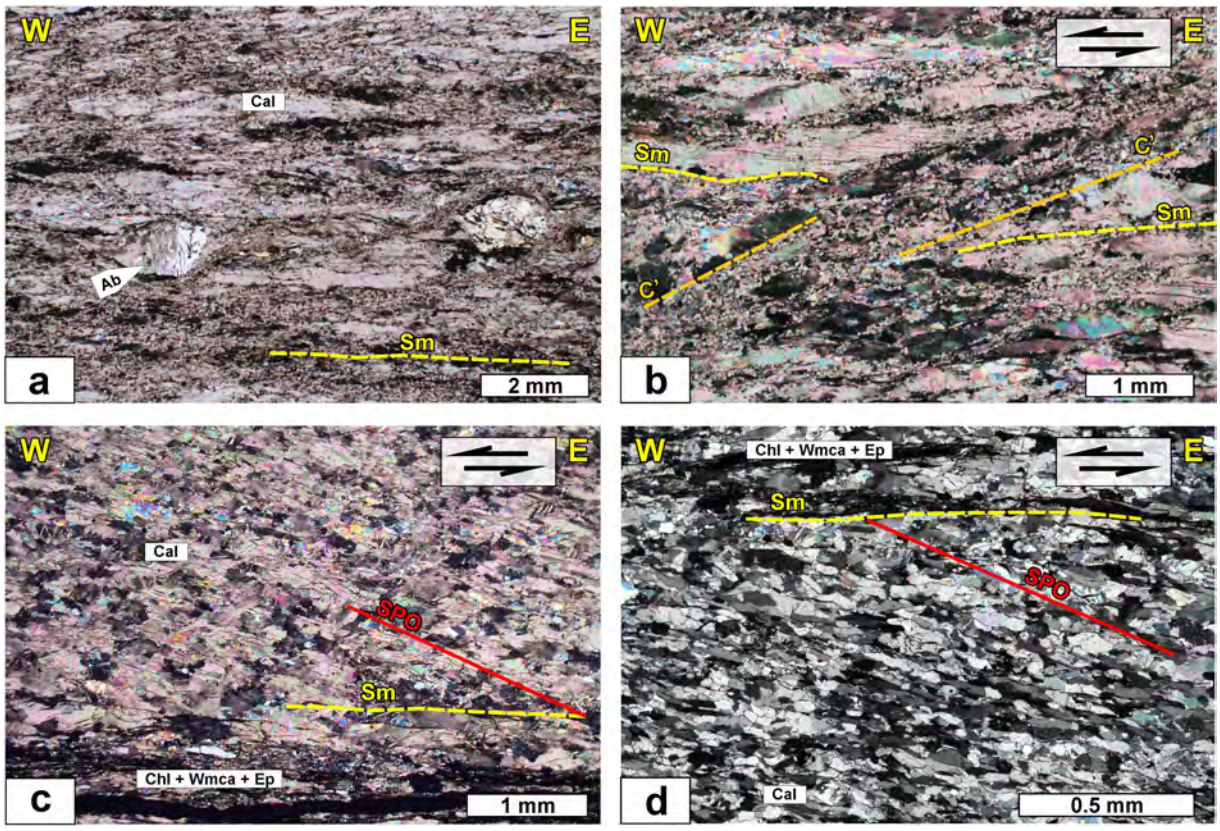

Figure 7. General microstructures. (a) Mylonitic microfabric showing rotated albite porphyroblasts surrounded by stretched and recrystallized calcite grains, defining the mylonitic foliation (S_m; CPL—Crossed polarized light). (b) Relic, coarse-grained calcite oriented parallel to the S_m, mantled by fine-grained, recrystallized calcite, and crosscut by top-to-the W C′ shear bands, associated with fine-grained calcite (CPL). (c and d) Examples of oblique foliation defined by the shape preferred orientation (SPO) of stretched calcite grains. Note the mylonitic foliation (S_m), highlighted by white mica + chlorite + quartz interlayers (CPL). Mineral abbreviations after Siivola and Schmid (2007).

phase that crystallized at blueschist-facies conditions. Its preferred orientation indicates a syn-kinematic origin with respect to the formation of S_m (Table 1). Chlorite occurs in gaps and pressure shadows around Na-amphibole and as Mn-rich grains in equilibrium with Na-amphibole rims (see Papeschi et al., 2020), indicating that it was present during greenschist- and part of the blueschist stages (Table 1). Na-amphibole occurs as prismatic and sigmoidal grains and mineral fishes (grain size: 0.1–1.0 mm) oriented and stretched parallel to the S_m (Figures 8a–8d). Sigmoidal grains typically display a zoning from a crossite core to an Mn-rich glaucophane-rim (Figures 8a and 8b), which was interpreted by Papeschi et al. (2020) to mark the breakdown of Mn-bearing phases close to the peak metamorphic grade. Zoning is commonly asymmetric, with glaucophane-rich rims forming at the stretched edges of Na-amphibole grains (Figures 8a and 8b). Na-amphibole is stretched and locally boudinaged along its basal cleavage, forming symmetric to asymmetric boudins with necks filled by calcite and quartz, as well as albite, titanite, and chlorite (Figures 8c and 8d). Although boudinage indicates that Na-amphibole is generally a pre-kinematic or relic phase with respect to the S_m (Table 1), the presence of sigmoidal glaucophane fish with asymmetric zoning patterns (Figures 8a and 8b) may suggest that these grains have also partly grown along the S_m during shearing.

Albite forms anhedral to euhedral syn-kinematic porphyroblasts up to 1–2 mm in size (Table 1; Figures 9a–9c). The S_m foliation is included and curved within albite porphyroblasts, where it is defined by oriented inclusions of calcite, quartz (Figures 9a and 9b), Na-amphibole (Figure 9c), white mica, chlorite, epidote (Figure 9d), and titanite. Its anticlockwise rotation with respect to S_m is consistent with a top-to-the W sense of shear. Na-amphibole and lawsonite pseudomorph inclusions in albite are partially to entirely resorbed and preserved as pseudomorphs (Figure 9c). Lawsonite pseudomorphs are commonly unoriented and clearly pre-kinematic (Figure 9d). The preservation of lawsonite only as epidote pseudomorphs in some albite

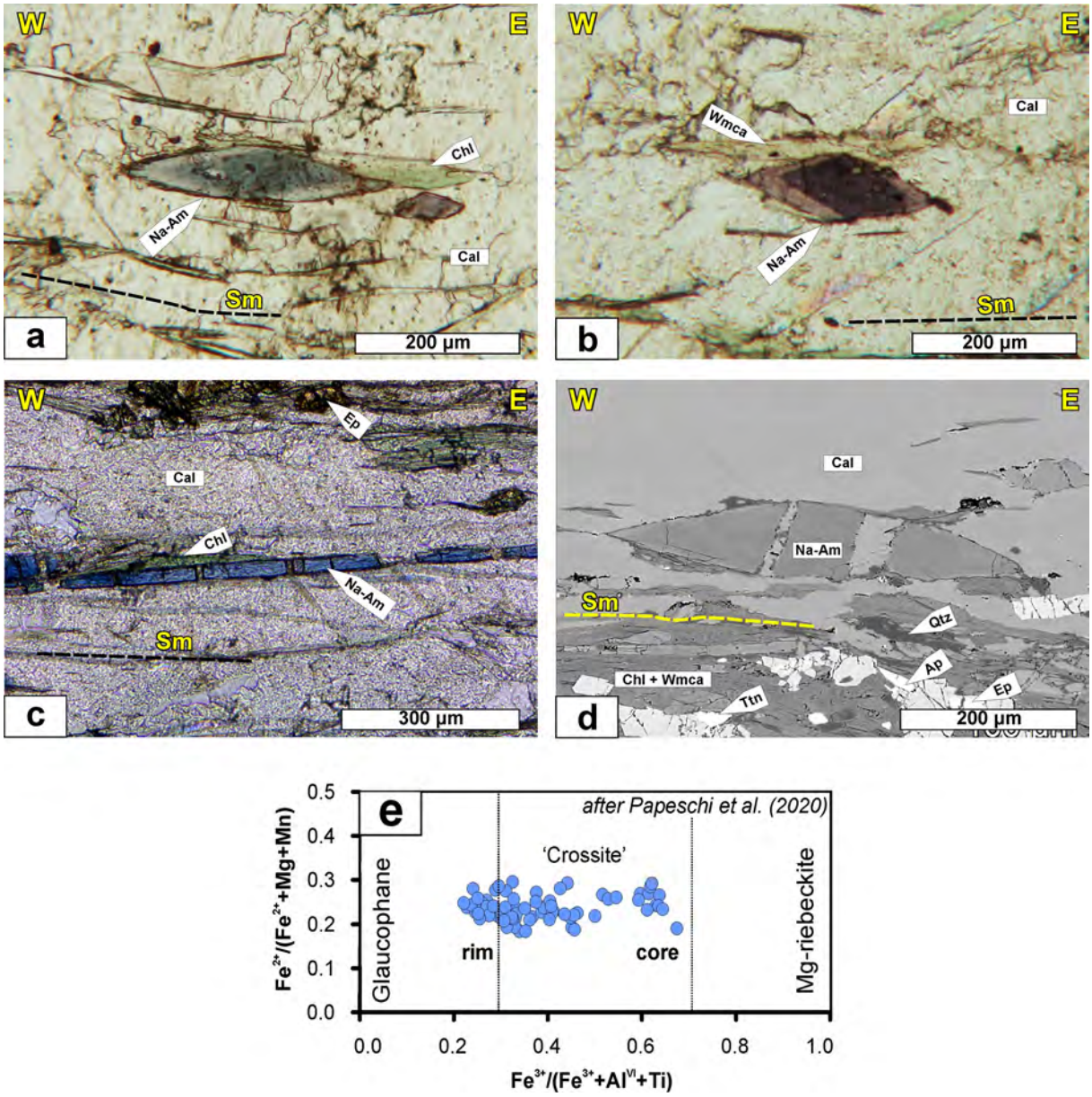

Figure 8. Deformation microstructures of Na-amphibole grains: (a and b) Examples of sheared Na-amphibole with sigmoidal shapes (mineral fish) surrounded by calcite and oriented white mica and chlorite grains, defining the S_m. Note the asymmetric mineral zoning transitioning from crossite in the core to glaucophane in the rim (details in Papeschi et al. [2020]; PPL—Plane polarized light). (c) Prismatic Na-amphibole grain boudins along the S_m foliation, marked by calcite, white mica, chlorite, and epidote (PPL). (d) Sigmoidal Na-amphibole grain boudins, with gaps filled by calcite + quartz, associated with chlorite, white mica, epidote, titanite, and apatite (BSE—Back scattered electrons). (e) Na-amphibole chemistry (modified after Papeschi et al. [2020]) showing the zoning from crossite (core) to glaucophane (rim), indicating a blueschist-facies metamorphic evolution. Mineral abbreviations after Siivola and Schmid (2007).

grains indicates that in the surrounding matrix this phase was likely destabilized and obliterated during mylonitic deformation.

The phyllosilicate-rich matrix contains euhedral to subhedral albite (grain size: 100–500 µm), epidote (10–200 µm), and titanite (10–100 µm) grains. In some cases, these grains contain gently rotated or deflected internal foliation planes (e.g., Figure 9e) and are, therefore, syn-kinematic with respect to the S_m. In others, they overgrow the S_m and lack evident pressure shadows and can thus be interpreted as post-kinematic (e.g., Figure 9f; Table 1). As shown by Papeschi et al. (2020), titanite sometimes occurs around relic, partially resorbed rutile grains that we interpret to have been stable at blueschist-facies (Table 1).

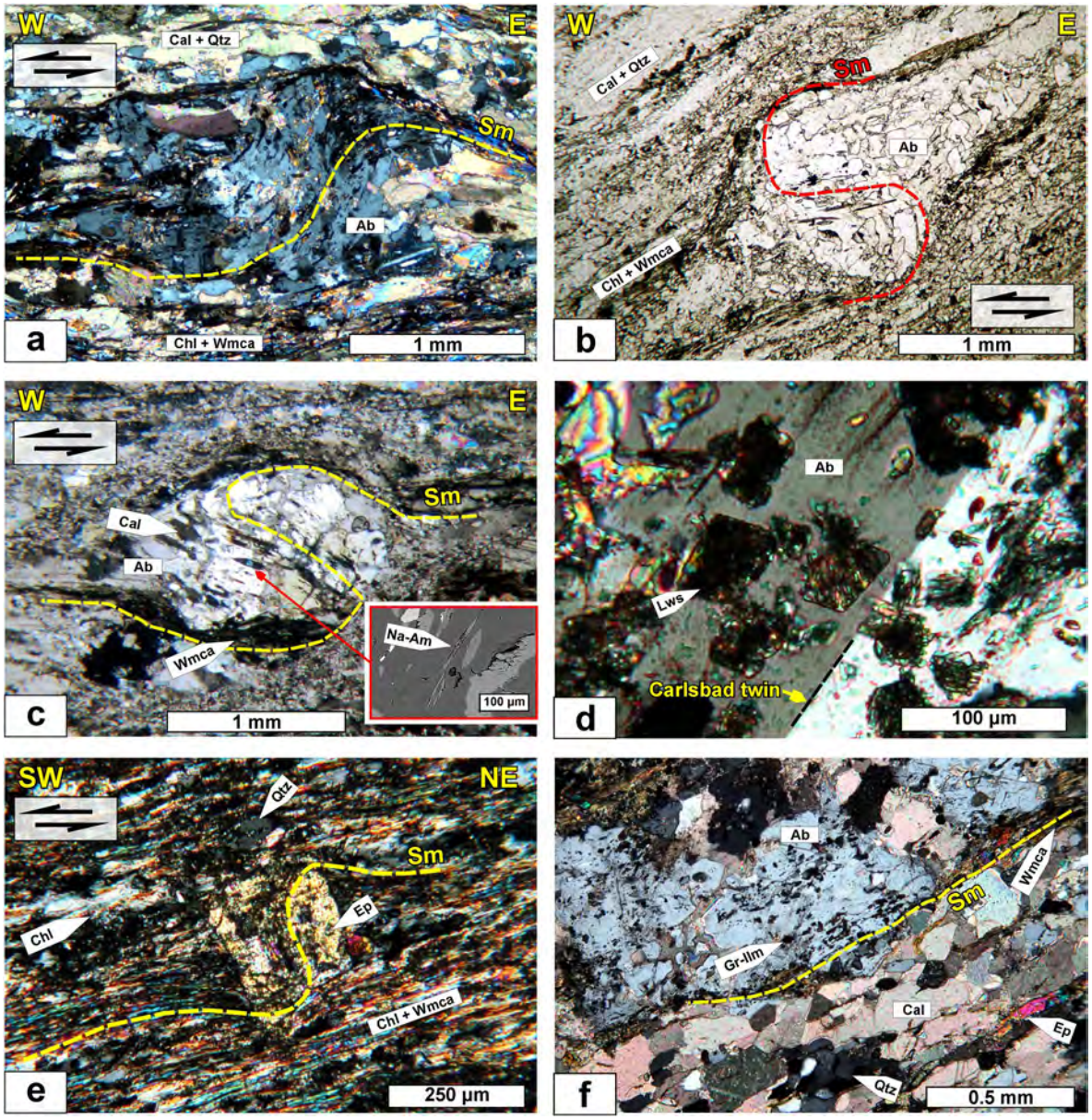

Figure 9. Albite Microstructures: (a and b) Examples of rotated albite porphyroblasts (syn-kinematic: see Passchier and Rudolph [2005]) with sigmoidal internal foliation, defined by oriented inclusions of white mica, chlorite, calcite, and quartz, continuous with the external S_m (a: CPL; b: PPL). (c) Detail of a rotated, syn-kinematic albite porphyroblast containing oriented inclusions of Na-amphibole (CPL). The insert shows a detailed BSE image of the Na-amphibole inclusions, partially resorbed by albite. (d) Detail of misoriented inclusions of lawsonite in albite (CPL). (e) Rotated epidote porphyroblast surrounded by white mica, chlorite, and quartz (CPL). The internal foliation is defined by tiny white mica and graphite inclusions. (f) Example of a post-kinematic albite grain with internal graphite-ilmenite trails continuous with the external foliation (CPL). Notice the lack of strain caps. Mineral abbreviations after Siivola and Schmid (2007).

5.4. EBSD Analysis

We used EBSD to generate spatially oriented data of the crystallographic preferred orientation (CPO) within the Acquadolce Subunit mylonitic calcschists. These data help to further describe the top-to-the W shear sense of these mylonites, but also to document their complex deformation history. The sample discussed herein (IESP3ERY21 A) is representative of the deformation style of all studied calc-mylonites. It is a mylonitic calcschist from the Rio Marina pier outcrop (Figure 3), where the HP-LT parageneses have been extensively documented (Bianco et al., 2015, 2019; Papeschi et al., 2020). At the outcrop and hand specimen scale, an overall ductile deformation style dominates and is associated with top-to-the W kinematic indicators (Figure 10a).

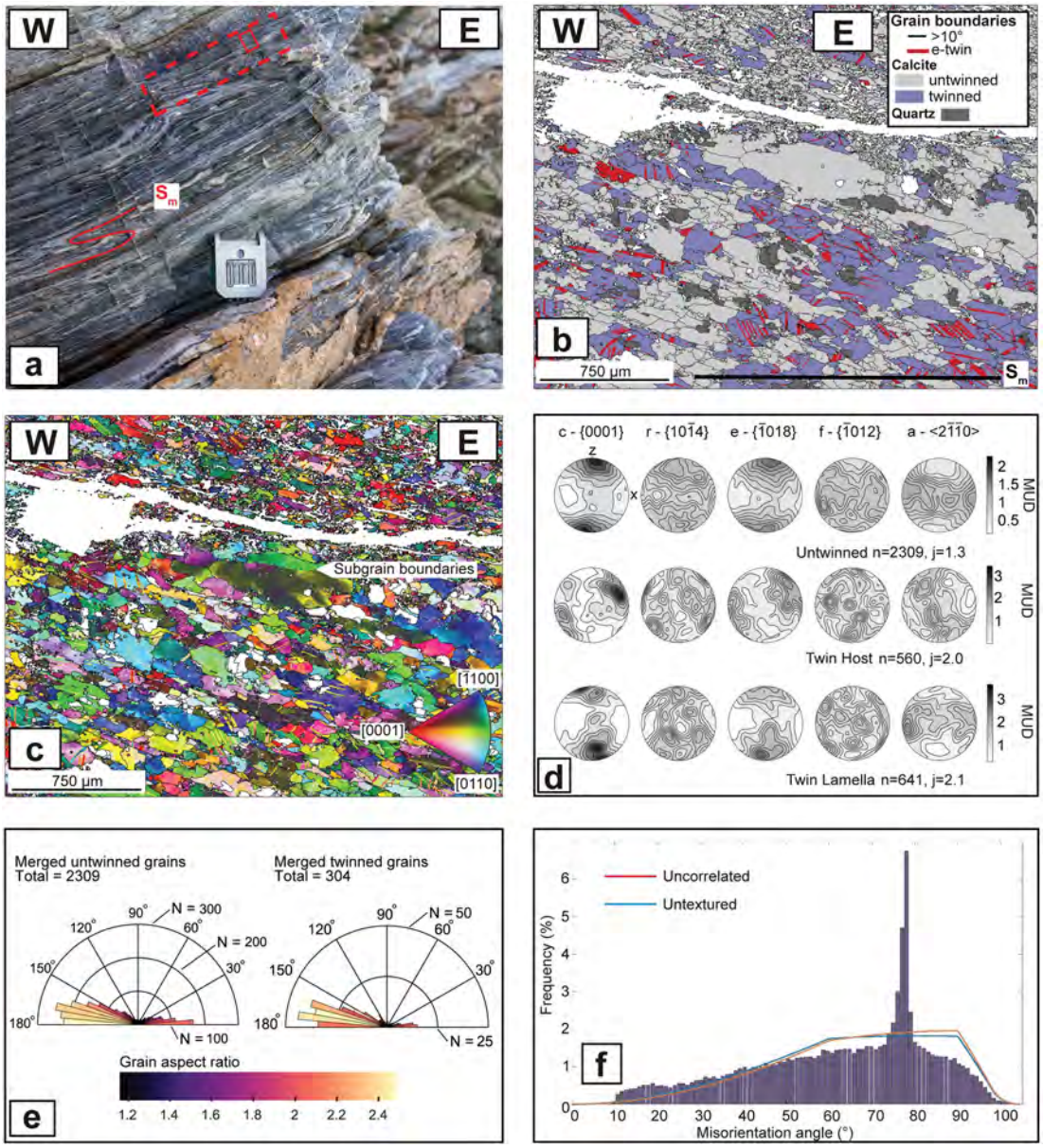

Figure 10. EBSD analysis. (a) Field photograph showing the location of the sample (dashed red box) and thin section (red box), as well as the folded mylonitic foliation (S_m). (b) Grain boundary map, showing twinned (purple) and untwinned (light gray) calcite grains, quartz grains (dark gray) and e-twin lamella (red). High-angle boundaries (misorientation threshold value: >10°) and interphase boundaries are shown in black. The white areas correspond to non-indexed phases (i.e., albite, white mica, chlorite, epidote, and titanite). The red stripes denote twin lamellae in the twinned calcite grains. (c) IPF map showing the orientation of grains and the presence of smaller sub-grains inside the larger calcite grains as indicated by variation in the IPF color (d) Contoured one-point-per-grain pole figures showing the distribution of c {0001}, r {10$\bar{1}$4}, e {$\bar{1}$018}, f {$\bar{1}$012} poles and a <2$\bar{1}\bar{1}$0> axis for the untwinned, twin host and twin lamellae calcite populations. J-index, after Bunge (1982). Contouring is shown as multiples of a uniform distribution (MUD). (e) Cumulative plot showing the distribution of the angle of calcite grains axes with respect to the horizontal (0–180°), parallel to the main foliation (Sm) for the untwinned and twinned calcite grain populations. The colored bars indicate the average aspect ratio of grains. (f) Misorientation angle distribution (MAD) for theoretically uncorrelated (red curve) and untextured (light blue curve) grains distribution. Blue histograms show the observed distribution.

The EBSD analysis was performed on a domain of dynamically recrystallized calcite characterized by a strong oblique SPO with respect to the S_m (Figure 10b). The resulting EBSD map is shown in Figure 10b, portraying calcite and quartz (dark gray) as indexed phases. We divided calcite grains into twin host (blue), twin lamellae (red), and untwinned (light gray) grain fractions. In total, 2,309 untwinned, 560 twin hosts, and 641 twin lamellae grains were indexed. Pole figures for the c {0001}, r {10$\bar{1}$4}, e {$\bar{1}$018}, f {$\bar{1}$012} poles and a <2$\bar{1}\bar{1}$0>

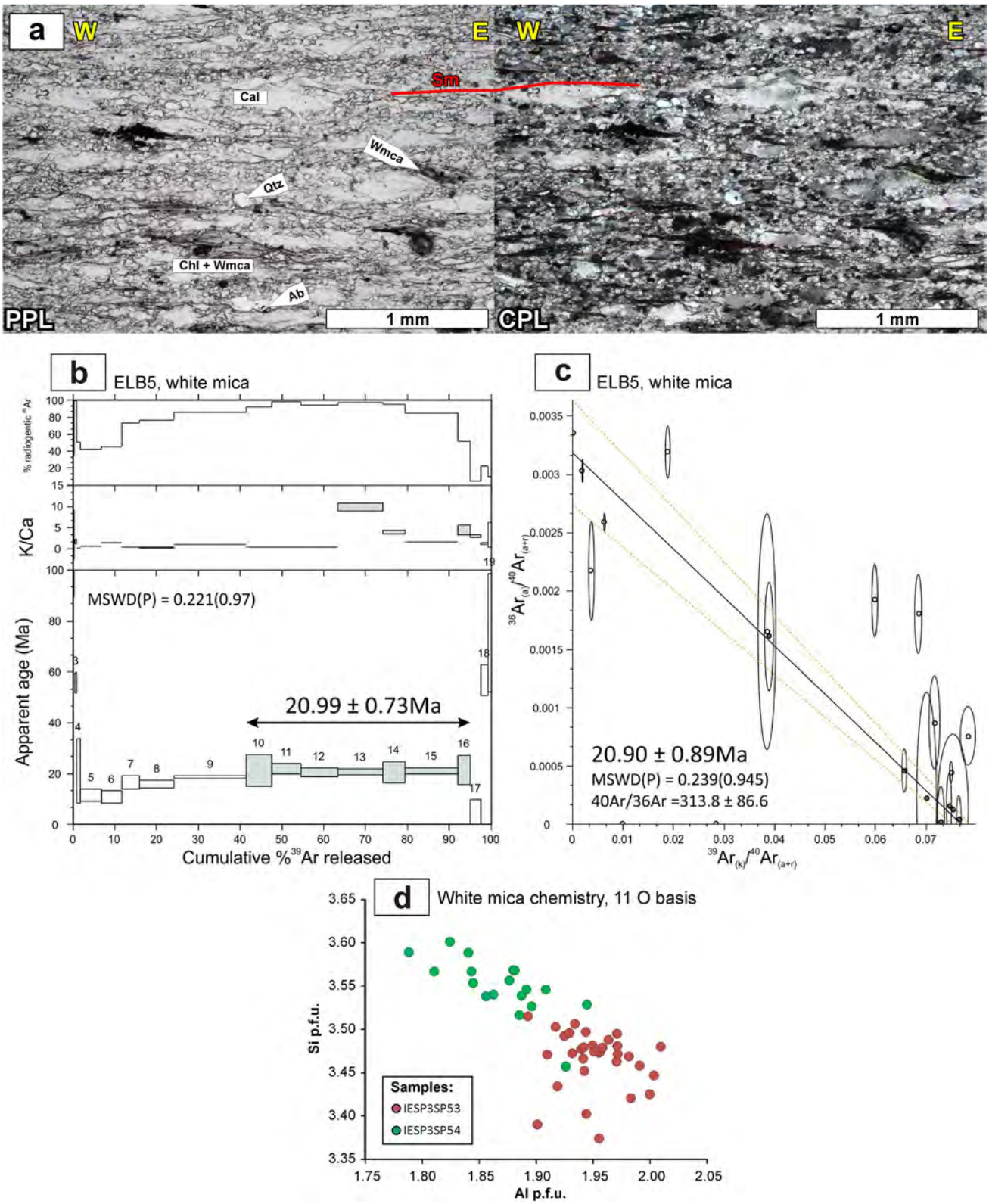
a
W
E
Cal
Sm
Wmca
Qtz
Chl + Wmca
Ab
PPL
1 mm
CPL
b
ELB5, white mica
% radiogentic ^{40}Ar
K/Ca
Apparent age (Ma)
MSWD(P) = 0.221(0.97)
20.99 ± 0.73Ma
Cumulative %^{39}Ar released
c
ELB5, white mica
$^{36}Ar_{(a)}/^{40}Ar_{(a+r)}$
20.90 ± 0.89Ma
MSWD(P) = 0.239(0.945)
40Ar/36Ar =313.8 ± 86.6
$^{39}Ar_{(k)}/^{40}Ar_{(a+r)}$
d
White mica chemistry, 11 O basis
Si p.f.u.
Al p.f.u.
Samples:
IESP3SP53
IESP3SP54

axis were generated as one-point-per-grain equal area, upper hemisphere projections, with X = lineation and Z = pole to the foliation orientations with respect to the finite strain ellipsoid reference frame (Figure 10d).

The mapped calcite grains have an average equivalent radius of 4.35 μm (p50 value) and exhibit lobate to ameboid grain boundaries (Figure 10b). Low-angle boundaries (misorientation threshold value: <10°) crosscut the calcite grains, dividing them into elongated sub-grains, as shown by varying IPF color within single grains (Figure 10c). The grains define a moderate SPO, inclined at 10°–15° to S_m, which is parallel to the bottom border of the frame (Figure 10b). The grains defining the SPO have an average aspect ratio of 2.0–2.5 and constitute most of the grain population. Grains oriented at high angle to S_m typically have a lower aspect ratio of *c*. 1.4–2.0 (Figure 10e). This inclined SPO is consistent with a top-to-the W sense of shear. Twinned grains are distributed throughout the sample, containing e-twins (approximate width 10 μm) oriented at large angles to S_m (Figure 10b). The high frequency of misorientation angles related to e-twinning is shown in Figure 10f.

The <c>-axis pole figures of the untwinned, twin host, and twin lamellae grain fractions are shown in Figure 10d. The distribution of the *c* <0001>-axis for the untwinned grain fraction defines a broad cluster around the pole to the S_m foliation (Z; Figures 10d) and 10a weak a $<2\bar{1}\,\bar{1}0>$ *a*-axis girdle distributed parallel to the XY foliation plane (Figure 10d). The <0001> *c*-axis maximum is only slightly rotated (10°–15°) in a clockwise direction with respect to and is roughly perpendicular to the SPO (Figure 10d). The CPO of the twin grains has been divided into host and lamellae fractions. The twin host grains define highly oblique *c*-axis girdle, rotated ∼60° clockwise from the pole to the S_m. The lamellae also have a strong *c*-axis maximum, but with a slight anticlockwise rotation of ∼10° from the pole to S_m. This is consistent with top-to-the E deformation via e-twinning (e.g., Schmid et al., 1987; Wenk et al., 1986), which occurs at low temperatures (i.e., <250°C–300°C; Burkhard, 1993; de Bresser & Spiers, 1993, 1997; Wenk et al., 1986). Neither the r- or f-poles of the host or lamellae fractions have a significantly preferred orientation, while the e-poles and *a*-axes of the lamellae show a weak, girdle-like CPO oriented normal and parallel to S_m, respectively (Figure 10d).

5.5. Geochronology

To obtain geochronological constraints on the exhumation of the Acquadolce Subunit, we collected one sample of calcschist (ELB5; Figures 11a) from the Rio Marina area for ^{40}Ar-^{39}Ar dating (Figures 11b and 11c; see Figure 3 and raw data in the supporting information). The sample is from the same Rio Marina pier outcrop where the EBSD sample was collected. There is no sign of contact metamorphism at this locality, which is also where peak HP-LT conditions were documented by Bianco et al. (2015, 2019) and Papeschi et al. (2020). Those authors reported celadonite-rich white mica with Si p.f.u. contents invariably above 3.00, up to 3.60 p.f.u. per 11 oxygens formula unit, a composition indicating HP metamorphism (Massonne & Schreyer, 1987; Massonne & Szpurka, 1997; Vidal & Parra, 2000). Phase equilibria modeling links the white mica phase to the $P > 1.5$ GPa mineral assemblage (Papeschi et al., 2020). We here report white mica compositional analyses from sample IESP3SP53 after Papeschi et al. (2020) and integrate them with analyses of a second sample (IESP3SP54) from the same part of the outcrop as ELB5 (Table S1). Analyses constrain an HP white mica with a Si p.f.u. content in the range of 3.30–3.60 and Al p.f.u. ∼1.80–2.00, based on 11 O basis (Figure 11d).

ELB5 is a strongly foliated calc-mylonite with relic calcite grains elongated parallel to S_m. Mantles of finer and dynamically recrystallized new grains surround the relic calcite grains (Figure 11a). Chlorite and white mica grains are aligned along the foliation planes and quartz and albite locally form sub-millimetric, sub-rounded clasts and elongated laths. The sample contains sigmoidal clasts and mica fish indicating top-to-the W kinematics (Figure 11a).

White mica in sample ELB5 yielded a 7-step $^{40}Ar/^{39}Ar$ plateau age at 20.99 ± 0.73 Ma (MSWD = 0.221; Figure 11b) corresponding to more than 50% of the cumulative released ^{39}Ar. The K/Ca ratios (calculated from $^{39}Ar_K/^{37}Ar_{Ca}$) over the concordant steps show some variation, but any potential age variations cannot be resolved in this analysis. The plateau age is in good agreement with the inverse isochron analysis (Fig-

Figure 11. Results of $^{40}Ar/^{39}Ar$ dating of sample ELB5 from the Rio Marina lighthouse: (a) General mylonitic microstructure of the sample, characterized by stretched, relic calcite, surrounded by recrystallized grains, and oriented white mica, chlorite, and albite grains (left: PPL; right: CPL). (b) Plot of the ELB 5 white mica $^{40}Ar/^{39}Ar$ data; % radiogenic ^{40}Ar, K/Ca ratio (calculated from $^{39}Ar_K/^{37}Ar_{Ca}$) and $^{40}Ar/^{39}Ar$ age spectrum, and (c) corresponding inverse isochron plot (20.90 ± 0.89 Ma). The trapped $^{40}Ar/^{36}Ar$ overlaps with the modern atmospheric value. (d) White mica chemistry from samples IESP3SP53 and IESP3SP54, from area A (Figure 4) plottred on Al p.f.u. – Si p.f.u. space, on 11 O basis.

ure 11c), which also precludes excess argon. We use the plateau age as the best age estimate of this sample in the following discussion.

6. Discussion

6.1. W-Verging Structures and Their Role During Exhumation

The presented structural, microstructural, EBSD, and geochronological data imply a tectonic history that we cannot readily reconcile with the existing post-orogenic exhumation models connected with the opening of the Northern Tyrrhenian Sea. Previous models specific to the Island of Elba suggested that exhumation of its metamorphic units occurred as part of an overall E-verging extensional structural framework, wherein initial top-to-the E thrusting was subsequently overprinted by top-to-the E syn- to post-orogenic low-angle normal faulting (e.g., Brunet et al., 2000; Collettini & Holdsworth, 2004; Jolivet et al., 1998; Keller & Coward, 1996).

While obviously maintaining that the E-vergence is fundamental within the nappe stack, we show that structures with typical Apenninic orientation in the Acquadolce Subunit (N-S to NW-SE striking and W-dipping foliation; Figure 4) diffusely also record W-directed shearing, that is, opposite to the first-order NE-directed thrusting kinematics that characterizes the Northern Apennines (e.g., Boccaletti et al., 1971; Keller & Coward, 1996). For the current orientation of the entire nappe stack within which the Acquadolce Subunit occurs, W-directed deformation corresponds to top-to-the W extensional shearing. We are not aware of any major, orogen-scale structure that may have caused large rotation of the nappe stack or parts thereof and therefore conclude that top-to-the W asymmetries represent overall extension. Although the evidence for this W-vergent kinematic framework is not ubiquitous and is also locally strongly overprinted, it needs to be accounted for in any model aiming to reconstruct the evolution of the area and, in turn, of the Northern Apennines.

We propose that exhumation of the Acquadolce Subunit may have initiated during a deformation phase including syn-orogenic, extensional top-to-the W shearing in a progressively forming E-verging nappe stack in the subduction channel. Indeed, many kinematic indicators in the Acquadolce Subunit are invariably consistent with top-to-the W deformation (Figures 6–9). Greenschist-facies assemblages are syn-kinematic with respect to the top-to-the W shearing and overprint mostly relic blueschist-facies parageneses that formed at peak metamorphic conditions. The general lack of kinematic indicators that can be directly ascribed to the initial HP evolution of the nappe stack inhibits the direct and confident link between blueschist-facies mineral phases and top-to-the W deformation. However, the widespread presence of celadonitic white mica defining the main foliation (Figure 11d; Papeschi et al., 2020) and independent documentation by Bianco et al. (2015, 2019) and the sigmoidal shape of Na-amphibole with asymmetric zoning patterns (Figures 8a and 8b), indicate that the early development of the exhumation-related S_m foliation started under blueschist-facies conditions.

The oblique foliation in the calc-mylonites, defined by a pervasive calcite SPO with respect to S_m (Figure 10e), is in agreement with top-to-the W kinematics. This sense of shear is possibly supported by the CPO of the untwinned calcite grains as indicated by the slight clockwise rotation of the *c*-axis maxima (Figure 10d; Rogowitz et al., 2014), although *c*-axis fabrics in calcite can be difficult to interpret with regards to the sense-of-shear (see the interpretations of Trullenque et al. [2006] vs. Rogowitz et al. [2014]). We interpret the e-twinning as evidence of later deformation, overprinting the earlier top-to-west fabric. This interperation is consistent with the lower temperatures documented for e-twinning in calcite (i.e., <250°C–300°C; Burkhard, 1993; de Bresser & Spiers, 1993, 1997; Wenk et al., 1986).

$^{40}Ar/^{39}Ar$ dating of celadonitic white mica from sample ELB5 sets a minimum age for the HP-LT parageneses to 20.99 ± 0.73 Ma (Figure 11b). This age is identical within error to the 19.8 ± 1.4 Ma $^{40}Ar/^{39}Ar$ age of syn-kinematic glaucophane from the same locality (Bianco et al., 2019) and the 19.68 ± 0.15 Ma $^{40}Ar/^{39}Ar$ age of white mica from the calcschist in the Rio Marina area (Deino et al., 1992). Bianco et al. (2019) associated the dated glaucophane with a retrograde metamorphic mineral assemblage, implying that their age constrains the ongoing exhumation of the HP-LT rocks. We also interpret our age to mark a post-HP metamorphic peak exhumation stage, likely the cooling below the closure temperature for the $^{40}Ar/^{39}Ar$ system in white mica. The maximum age for HP metamorphism can be constrained to 31.6 ± 0.5 Ma (e.g., Jacobs et al., 2018), which is the maximum deposition age of the youngest deposits that were subject to blueschist-facies metamorphism.

According to Papeschi et al. (2020), the exhumation of the HP-LT blueschists of the Acquadolce Subunit occurred at nearly isothermal conditions from peak conditions at 1.5–1.8 GPa and 320°C–370°C. Isothermal decompression occurred between 21–19 Ma (HP-LT metamorphism) and 6–7 Ma (contact metamorphism at 0.2 GPa; Musumeci et al., 2015) at very fast exhumation rates (2.5–3.7 km/Ma; see Papeschi et al., 2020). Such a cold exhumation path is consistent with syn-orogenic exhumation (see also Rossetti et al., 2002). Therefore, we suggest that during the Oligocene–early Miocene W-verging extensional structures within the east-verging and west-dipping Northern Apennines nappe stack played a significant role in exhuming deep metamorphic units from blueschist- to greenschist-facies conditions.

6.2. Extrusion Model of the Acquadolce Subunit: Implications for Exhumation of HP-LT Units in the Northern Apennines

The Northern Apennines contain several arcuate, antiform-to dome-like structures, the cores of which consist of metamorphic rocks currently cropping out below subgreenschist-facies units (Figure 1a). These geological features were initially interpreted as metamorphic core complexes (Carmignani & Kligfield, 1990), and exhumation was proposed to have mainly occurred during syn- to post-orogenic extension in the footwall of major, E-verging low-angle normal faults that bound the complexes (Carmignani et al., 1994, 2001, 2004; Daniel & Jolivet, 1995; Jolivet et al., 1998; Rossetti et al., 1999; Pauselli et al., 2006). HP-LT parageneses with peak pressure >1.0 GPa therein (Theye et al., 1997; Giorgetti et al., 1998; Rossetti et al., 1999) have, however, challenged the post-orogenic extension model. Jolivet et al. (1998) and Rossetti et al. (2002), who argued that the exhumation was accommodated by post-orogenic back-arc extension, thus also suggested that HP-LT metamorphic rocks had in part been exhumed along cold geothermal gradients, typical of syn-orogenic exhumation paths. Such a two-stage evolution is supported by data from the Alpi Apuane area (Figure 1a), where "cold," syn-orogenic exhumation occurred between 25 and 13 Ma, while the overlying Tuscan Nappe was still being underthrusted (Fellin et al., 2007; Molli et al., 2018). In the Alpi Apuane, higher-grade rocks of the Massa Unit ($P > 0.8$ GPa) are structurally above lower-grade units (Apuane Unit; $P \sim 0.4$–0.6 GPa), suggesting that the Massa Unit was thrust onto the Apuane Unit at some stage during exhumation (Carosi et al., 2004; Jolivet et al., 1998; Molli et al., 2000). W-verging folds in the area were also interpreted to have formed during exhumation (Molli et al., 2000; Storti, 1995).

Despite this first-order evidence, the mechanisms and structures driving and accommodating syn-orogenic exhumation have proved difficult to document and remain largely unexplored and unaccounted for in the Northern Apennines belt. The data presented here constrain instead widespread W-verging extensional shearing within overall E-vergent thrust nappes in the Tyrrhenian sector of the belt, accommodating exhumation of the Acquadolce Subunit, likely from blueschist-to greenschist-facies conditions. Due to its minor structural thickness of just 500–700 m, the Acquadolce Subunit only represents one slice of HP-LT rocks preserving evidence of early, W-verging structures within the orogenic wedge, which was largely reworked by Late Miocene tectonics and magmatism. We argue that W-directed extension was coeval with E-directed thrusting, thus driving the exhumation of the Acquadolce Subunit by ductile extrusion from blueschist-to greenschist-facies conditions in an overall contractional setting (e.g., Law et al., 2006; Ring & Glodny, 2010; Ring, Glodny, et al., 2007; Ring, Will, et al., 2007; Searle, 2010; Lamont et al., 2019). Exhumation by syn-orogenic extrusion is supported by the nearly isothermal P-T path recorded by the Acquadolce Subunit (see Papeschi et al., 2020) and similar units in the region (Jolivet et al., 1998; Rossetti et al., 1999, 2001, 2002). Extrusion may also have exhumed the Ortano and Calamita Units from HP-LT conditions. However, late Miocene LP-HT contact metamorphism therein has largely obliterated older assemblages and structures and the early Miocene-Oligocene metamorphic peak conditions experienced by the Ortano and Calamita Units remain unknown. The common top-to-the E thrusts and multiscalar asymmetries that pervasively define the current upper and lower boundaries of the Acquadolce Subunit are significantly younger than the peak HP-LT paragenesis (Musumeci et al., 2015; Viola et al., 2018) and are coeval with Porto Azzurro monzogranite-related contact metamorphism at $P < 0.2$ GPa (Musumeci & Vaselli, 2012). As such, they represent late orogenic structures and cannot be directly associated with the W-vergent geological record presented here.

Based on existing and our new structural and metamorphic data, we propose an evolutionary scheme for the Acquadolce Subunit that has the potential to account for the syn-orogenic exhumation of HP-LT rocks in this portion of the inner Northern Apennines. We implement our constraints in a model that integrates

the geodynamic evolution for the Northern Apennines proposed by Bonini et al. (2014; Figure 12) and use our results to better constrain the processes that took place in the subduction channel at depths between ca. 50 and 20 km from the late Oligocene to the late Miocene (Figure 12). According to Bonini et al.'s model, the overall late Oligocene-late Miocene evolution shown in Figures 12a–12c can be placed within a framework of progressive Adria slab roll-back, retreat, and delamination. However, in the context of regional upper-plate extension associated with this evolution, late Miocene crustal shortening (Figure 12c) would have ensued in response to a transient stop in the subduction process. Such a stop would have allowed for coupling between the upper and lower plates causing the transfer of compression to the formerly extending upper plate, including the Northern Apennines hinterland and the Tyrrhenian back-arc basin. Viola et al. (2018) have indeed documented compressional pulses in the late Miocene on the Island of Elba.

The documented tectonic history of the Acquadolce Subunit can be readily framed into this regional picture by referring to the three conceptual stages described by Bonini et al. (2014), as shown in Figure 12. (1) During the late Oligocene-early Miocene, the Acquadolce Subunit was subducted to depths corresponding to 1.5–1.8 GPa by deep underplating beneath the early Apennine orogenic wedge. In our model, this occurred under overall compression during the structuring of the orogenic wedge through nappe stacking (Figure 12a and detail of the subduction channel); (2) during the early middle Miocene (Figures 12a and 12b) the Acquadolce Subunit experienced partial exhumation by syn-orogenic extrusion within the subduction channel to shallower crustal levels, driven by the W-verging structures at the top, documented here, and the inferred E-verging structures at the bottom. This stage likely occurred at *c*. 19–21 Ma (minimum age of HP-LT metamorphism), and certainly before 6–7 Ma, the age of the Porto Azzurro contact metamorphic overprint at 0.2 GPa. Assuming that exhumation occurred in this age interval, exhumation rates can be constrained to *c*. 2.5–3.7 km/Ma. We propose that while exhumation at depth was by upward extrusion within an overall contractional setting, extension dominated the uppermost wedge, which was responding to the dynamics of the critical taper (e.g., Massa et al., 2017); (3) in the late Miocene, the hinterland was recompressed and deformation was mostly accommodated by E-verging thrusts within the orogenic wedge leading to final nappe stacking (Figure 12c). This late Miocene event (Massa et al., 2017) is constrained by direct dating of thrusts and syn-kinematic contact metamorphism down to at least 6 Ma (Musumeci et al., 2015; Viola et al., 2018) and occurred at $P < 0.2$ GPa (Musumeci & Vaselli, 2012).

In this reconstruction, we do not show the Zuccale Fault, whose brittle top-to-the E shearing was dated to < 6 Ma (Viola et al., 2018), after the end of the time window considered in this study.

According to our model, the reconstructed structural and metamorphic evolution of the Acquadolce Subunit occurred entirely in an overall contractional scenario, with syn-orogenic extrusion followed by late Miocene thrusting, leading to the incorporation of HP-LT metamorphic units into the shallower portions of the orogenic wedge. Extension occurred in the middle Miocene, but we exclude that it played a major role in the exhumation of the HP units studied here.

In light of similar "cold" exhumation P-T paths recorded by other HP-LT units in the Northern Apennines (e.g., Jolivet et al., 1998; Rossetti et al., 1999, 2002; Theye et al., 1997), we propose that syn-orogenic extrusion facilitated by distributed W-verging extensional shearing was not only limited to the Island of Elba, but possibly played an important role to facilitate the exhumation of other metamorphic units in the Tyrrhenian sector of the belt (e.g., Gorgona, Giglio and Argentario; e.g., Brogi & Giorgetti, 2012; Giorgetti et al., 1998; Jolivet, 1998; Rossetti et al., 1999, 2001; Theye et al., 1997). Indeed, a belt of partially preserved HP-LT metamorphic rocks in the Northern Tyrrhenian Sea can be traced from the Island of Gorgona in the north through the Island of Elba to the Island of Giglio and the Argentario Promontory in the south. These HP-LT rocks may testify to the importance of syn-orogenic extrusion in the innermost portion of the Northern Apennines. The effective thickness of the extruding HP-LT unit might therefore be significantly larger than that of the Acquadolce Subunit. The base of a thicker extruding unit may be defined by E-vergent thrusts, coeval to and with a similar metamorphic grade to the extensional W-vergent fabrics described here. Considering the geometry of the HP-LT metamorphic rocks in the Northern Tyrrhenian Sea, the true base of the extruding HP-LT unit is likely located farther east, toward the Italian mainland. Although more accurate radiometric data are needed to better constrain HP-LT events in the Northern Apennines, the data presented here suggest that the Adria continental margin, together with remnants of the Ligurian Ocean, was

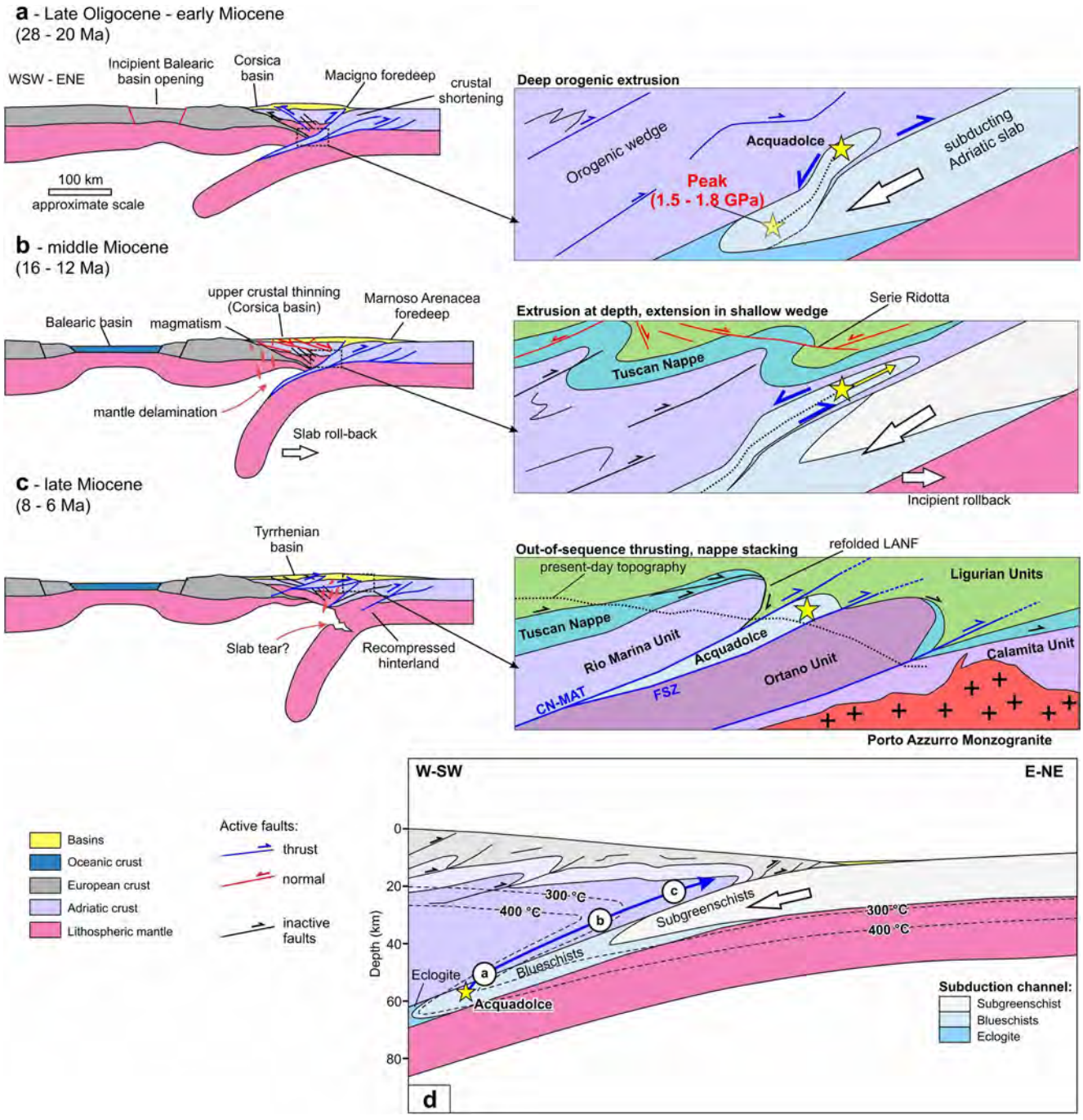

Figure 12. (a–c) Geodynamic model for the evolution of the Northern Tyrrhenian back-arc basin and the Northern Apennines for the late Oligocene-late Miocene time interval, modified from Bonini et al. (2014). The sketches of the processes within the subduction channel (not to scale) illustrate the tectonic and exhumation history of the Acquadolce Subunit within the Northern Apennines orogenic wedge in the late Oligocene-late Miocene time interval. (a) Subduction and deep underthrusting. (b) Exhumation by syn-orogenic extrusion within overall contraction at deep structural levels of the orogenic wedge and extension in the upper orogenic wedge in response to the dynamics of the critical taper. (c) Thrusting after exhumation to shallow crustal levels. See the discussion for further details. (d) P-T framework of the Northern Apennines subduction channel. Circles a, b, and c refer to the conditions experienced by the Acquadolce subunit during its progressive exhumation path from blueschist-to greenschist facies conditions from the late Oligocene–early Miocene (a) to the middle Miocene (b) and the late Miocene (c). See the text for further details.

involved in the late Oligocene-early Miocene W-dipping subduction, after the Eocene continental collision in the Western Alps-Alpine Corsica.

7. Conclusions

We have conducted a detailed structural analysis of the Acquadolce Subunit, a tectonic sliver preserving an HP-LT signature within the Eastern Elba nappe stack. Our results show, for the first time, that diffuse top-to-the W extensional shearing affected the subunit as it was being incorporated into the progressively growing orogenic wedge characterized by an overall E-vergence. The documented top-to-the W extensional shearing allowed the overall upward extrusion of the Acquadolce Subunit as a discrete sliver. The subunit's exhumation relative to the surroundings involved its detachment from the subducting slab and upward migration within the subduction channel during continued subduction. Transition from peak blueschist conditions of 1.5–1.8 GPa and 320°C–370°C at least *c*. 21–19 Ma ago to greenschist-facies conditions reflects localized exhumation through ductile extrusion in the overall contractional setting of the Apennines orogenic wedge, such that the documented exhumation is purely syn-orogenic. Late Miocene, E-verging compressive tectonics, contact metamorphism, and later extension reworked the wedge to its current complex geometric configuration, obliterating much of the evidence supporting exhumation by extrusion during the early stages of wedge build-up.

Future research needs to be directed toward determining whether the mechanism proposed for the local exhumation of the Acquadolce Subunit can be realistically applied to other HP-LT metamorphic units of the inner Apennines belt. It is increasingly accepted that no single exhumation mechanism controls the exhumation style of any particular tectonic domain. Local geological peculiarities may lead to exhumation accommodated by structural styles that change in space and time within the same subduction system. More multidisciplinary studies combining detailed structural, petrological, and thermo-geochronological data are needed to explain the occurrence of HP-LT units in the inner Apennines, where it is clear that post-orogenic extension cannot account for all exhumation.

Many of the complexities on the Island of Elba are due to the Late Miocene intrusions of the Tuscan Magmatic Province, which have partly fully overprinted the geological record of the early stages of exhumation. Studies of HP-LT units elsewhere in the belt may thus be even more telling about the early increments of their exhumation path.

Appendix A: EBSD Analysis

Selected samples were chemically polished using an OP-U, 400Å suspended colloidal silica polishing agent and rinsed in 96% alcohol (Moen et al., 2003). Samples were mounted on metal mounting pedestals, at the standard eccentric height, using a tilt angle of 70° with respect to the horizontal (Prior et al., 2009) and a working distance of 21.9 mm. To avoid geometric trapezoidal scan distortions in the collected maps, a correction to the beam scan voltages was implemented using a gridded standard calibration (Sørensen et al., 2020). To acquire optimal EBSD patterns, the SEM vacuum was set on a variable pressure mode, low vacuum setting, and an accelerating voltage of 20 keV, using an extraction voltage of 1.70 kV and open apertures. EBSD patterns were acquired with the NORDIF UF-1000 detector (Chen et al., 2012) using a 240 × 240 pixel resolution and the NORDIF 3.0 software for pattern acquisition. The samples were analyzed using a step size of 2 μm to allow for the mapping of large areas and a significant number of grains. Acquisition and calibration patterns were selected in the corners and at the center of the scan area using the NORDIF interface and electron image, to calibrate the pattern center across the large area scans.

The data were processed using the open-source Matlab toolbox MTEX 5.2.2 (Bachmann et al., 2010, 2011; Mainprice et al., 2015). Noise reduction was performed to eliminate mis-indexed points and artifacts. During indexing, grain boundaries between calcite grains are often misinterpreted as dolomite (Sørensen et al., 2020). Therefore, we removed false dolomite grains. During grain reconstruction, unindexed areas less than 20 pixels in area were ignored to avoid tiny holes inside the calculated grains. The threshold for high-angle grain boundaries was set at 10°.

We used the hexagonal unit cell with cell parameters $c = 17.064$ Å and $a = b$ 4.99 Å to index the calcite EBSD data. E-twin boundaries were identified as grain boundaries, when the angle between either of the two ideal e-twins and observed misorientations was less than 8°. The definition of the e-twin is the reflection across the {−1 0 1 8} plane, which in EBSD translates to the rotation operation of 78.1083° around either the (1 −1 0 4) or the (0 1 −1 4) poles. To differentiate twin lamellae and host grains, we used MTEX grain shape parameters. The widest host grain lamella was selected as the host seed. The other host lamellae were then selected based on their misorientation to the host seed (<15°). The lamella with a misorientation to the host seed of less than 15° from the ideal e-twin misorientation was then classified as e-twin lamella.

Appendix B: $^{40}Ar/^{39}Ar$

The selected sample was crushed and sieved to obtain 180–250 and 80–120 μm grain fractions. Finer particles were decanted in tap water, while the coarser residue was treated with several ultrasonic baths in acetone and deionized water. The optically best grains, void of any coating, were handpicked under a microscope. The grains were packed in aluminum capsules together with a Taylor Creek Rhyolite (TCR) flux monitor standard along with zero age reagent grade K_2SO_4 and optical grade CaF_2 salts for interference corrections. The sample was irradiated at IFE (Institutt for Energiteknikk) for about 70 h, with a nominal neutron flux density of *c.* 1.3×10^{13} n × ($cm^{-2} \times s^{-1}$). The sample was placed in a 3.5 mm pit size aluminum sample disk and step heated using a defocused 3.5 mm CO_2 laser beam from Photon Machine Fusions 10.6 with a flat energy spectrum. The gases extracted from the sample cell were expanded into a Piston Free Stirling Cryocooler to trap potential water into a two-stage low volume extraction line (*c.* 300 cm^3). Both stages were equipped with SAES GP-50 (st101 alloy) getters, the first running hot (*c.* 350°C) and the second running cold. They were analyzed with a MAP 215–50 mass spectrometer in static mode, installed at the Geological Survey of Norway. The peaks and baseline (AMU = 36.2) were determined during peak hopping for 10 cycles (15 integrations per cycle, 30 integrations on mass ^{36}Ar) on the different masses ($^{40–36}Ar$) on a Balzers SEV 217 electron multiplier in analog mode and regressed back to zero inlet time. Blanks were analyzed for every third measurement. After blank correction, a correction for mass fractionation, ^{37}Ar and ^{39}Ar decay and neutron-induced interference reactions produced in the reactor was undertaken using in-house software AgeMonster, written by M. Ganerød. The software implements the equations of McDougall and Harrison (1999) and the newly proposed decay constant for ^{40}K after Renne et al. (2010). A $^{40}Ar/^{36}Ar$ ratio of 298.56 ± 0.31 from Lee et al. (2006) was used for the atmospheric argon correction and mass discrimination calculation using a power law distribution of the masses. We calculated *J*-values relative to an age of 28.619 ± 0.036 Ma for the TCR sanidine flux monitor (Renne et al., 2010). We define a plateau according to the following requirements: at least three consecutive steps overlapping at the 95% confidence level (1.96σ) using the strict test:

$$overlap\ if\ : abs\left(age_n - age_{n+1}\right) < 1.96\sqrt{\left(\sigma_n^2 + \sigma_{n+1}^2\right)}\ \text{(if errors quoted at 1}\sigma\text{)},$$

≥50% cumulative ^{39}Ar released, and mean square of weighted deviates (MSWD) less than the two-tailed student *T* critical test statistics for $n - 1$. Weighted mean ages are calculated by weighting on the inverse of the analytical variance. The uncertainties are expanded in cases where MSWD > 1 using $\sigma * \sqrt{MSWD}$ to account for this excess error contribution.

Acknowledgments
The authors wish to thank Paolo S. Garofalo for financially supporting Samuele Papeschi during some of his fieldwork in the area and for constructive feedback. The authors are indebted to Gianluca Vignaroli and Francesco Giuntoli (Università di Bologna) for many constructive discussions in the field and in the office on the metamorphic complexes of the Northern Apennines and on the mechanisms steering their exhumation. Critical and constructive reviews by two anonymous reviewers, Michele Zucali, Alberto Vitale Brovarone, Associate Editor Federico Rossetti, and Editor Laurent Jolivet, have contributed to a much-improved final version of the study.

Data Availability Statement

Data sets and Supporting Information can be accessed at Viola, Giulio (2021), "Ryan et al., 2021", Mendeley Data, V2, http://dx.doi.org/10.17632/bj3nwk3wpm.2.

References

Agard, P., Yamato, P., Jolivet, L., & Burov, E. (2009). Exhumation of oceanic blueschists and eclogites in subduction zones: Timing and mechanisms. *Earth-Science Reviews*, *92*(1–2), 53–79. https://doi.org/10.1016/j.earscirev.2008.11.002

Avigad, D., Garfunkel, Z., Jolivet, L., & Azañón, J. M. (1997). Back arc extension and denudation of Mediterranean eclogites. *Tectonics*, *16*(6), 924–941. https://doi.org/10.1029/97tc02003

Bachmann, F., Hielscher, R., & Schaeben, H. (2010). Texture analysis with MTEX – Free and open source software toolbox, *Solid State Phenomena*, *160*, 63–68. https://doi.org/10.4028/www.scientific.net/ssp.160.63

Bachmann, F., Hielscher, R., & Schaeben, H. (2011). Grain detection from 2d and 3d EBSD data—Specification of the MTEX algorithm. *Ultramicroscopy*, *111*(12), 1720–1733. https://doi.org/10.1016/j.ultramic.2011.08.002

Barboni, M., Annen, C., & Schoene, B. (2015). Evaluating the construction and evolution of upper crustal magma reservoirs with coupled U/Pb zircon geochronology and thermal modeling: A case study from the Mt. Capanne pluton (Elba, Italy), *Earth and Planetary Science Letters*, *432*, 436–448.

Beaumont, C., Jamieson, R. A., Nguyen, M. H., & Lee, B. (2001). Himalayan tectonics explained by extrusion of a low-viscosity crustal channel coupled to focused surface denudation. *Nature*, *414*, 738–742. https://doi.org/10.1038/414738a

Behr, W. M., & Platt, J. P. (2012). Kinematic and thermal evolution during two-stage exhumation of a Mediterranean subduction complex. *Tectonics*, *31*(4). https://doi.org/10.1029/2012tc003121

Berthé, D., Choukroune, P., & Jegouzo, P. (1979). Orthogneiss, mylonite and non coaxial deformation of granites: The example of the South Armorican Shear Zone. *Journal of Structural Geology*, *1*(1), 31-42.

Bianco, C., Brogi, A., Caggianelli, A., Giorgetti, G., Liotta, D., & Meccheri, M. (2015). HP-LT metamorphism in Elba Island: Implications for the geodynamic evolution of the inner Northern Apennines (Italy). *Journal of Geodynamics*, *91*, 13–25. https://doi.org/10.1016/j.jog.2015.08.001

Bianco, C., Godard, G., Halton, A., Brogi, A., Liotta, D., & Caggianelli, A. (2019). The lawsonite-glaucophane blueschists of Elba Island (Italy). *Lithos*, *348–349*, 105198. https://doi.org/10.1016/j.lithos.2019.105198

Boccaletti, M., Corti, G., & Martelli, L. (2011). Recent and active tectonics of the external zone of the Northern Apennines (Italy). *International Journal of Earth Sciences*, *100*(6), 1331–1348. https://doi.org/10.1007/s00531-010-0545-y

Boccaletti, M., Elter, P., & Guazzone, G. (1971). Plate tectonic models for the development of the Western Alps and Northern Apennines. *Nature Physical Science*, *234*(49), 108–111. https://doi.org/10.1038/physci234108a0

Bonini, M., & Sani, F. (2002). Extension and compression in the Northern Apennines (Italy) hinterland: Evidence from the late Miocene-Pliocene Siena-Radicofani Basin and relations with basement structures. *Tectonics*, *21*(3), 1. https://doi.org/10.1029/2001tc900024

Bonini, M., Sani, F., Stucchi, E. M., Moratti, G., Benvenuti, M., Menanno, G., & Tanini, C. (2014). Late Miocene shortening of the Northern Apennines back-arc. *Journal of Geodynamics*, *74*, 1–31. https://doi.org/10.1016/j.jog.2013.11.002

Bortolotti, V., Fazzuoli, M., Pandeli, E., Principi, G., Babbini, A., & Corti, S. (2001). Geology of central and eastern Elba Island, Italy. *Ofioliti*, *26*(2A), 97–150.

Bouillin, J. P. (1983). Examples of deformations connected with intrusions of alpine granitoids in distentional conditions: The Elba Island (Italy) and the Cap Bougaroun (Algeria). *Revue de géologie dynamique et de géographie physique Paris*, *24*(2), 101–116.

Brogi, A., & Giorgetti, G. (2012). Tectono-metamorphic evolution of the siliciclastic units in the Middle Tuscan Range (inner Northern Apennines): Mg-carpholite bearing quartz veins related to syn-metamorphic syn-orogenic foliation. *Tectonophysics*, *526–529*, 167–184. https://doi.org/10.1016/j.tecto.2011.09.015

Brunet, C., Monié, P., Jolivet, L., & Cadet, J.-P. (2000). Migration of compression and extension in the Tyrrhenian Sea, insights from $^{40}Ar/^{39}Ar$ ages on micas along a transect from Corsica to Tuscany. *Tectonophysics*, *321*(1), 127–155. https://doi.org/10.1016/s0040-1951(00)00067-6

Bunge, H. (1982). *Texture analysis in materials science: Mathematical models*. Butterworths.

Burkhard, M. (1993). Calcite twins, their geometry, appearance and significance as stress-strain markers and indicators of tectonics regime: A review. *Journal of Structural Geology*, *15*(3–5), 351–368. https://doi.org/10.1016/0191-8141(93)90132-t

Carmignani, L., Conti, P., Cornamusini, G., & Meccheri, M. (2004). *The internal Northern Apennines, the northern Tyrrhenian Sea and the Sardinia-Corsica block*. Geology of Italy. Special Volume, Italian Geological Society, IGC.

Carmignani, L., Decandia, F. A., Disperati, L., Fantozzi, P. L., Kligfield, R., Lazzarotto, A., et al. (2001). Inner northern Apennines. In G. B. Vai, & I. P. Martini, (Eds.), *Anatomy of an orogen: The Apennines and adjacent Mediterranean basins* (pp. 197–214).

Carmignani, L., Decandia, F. A., Fantozzi, P. L., Lazzarotto, A., Liotta, D., & Meccheri, M. (1994). Tertiary extensional tectonics in Tuscany (northern Apennines, Italy). *Tectonophysics*, *238*(1–4), 295–315. https://doi.org/10.1016/0040-1951(94)90061-2

Carmignani, L., & Kligfield, R. (1990). Crustal extension in the Northern Apennines: The transition from compression to extension in the Alpi Apuane core complex. *Tectonics*, *9*(6), 1275–1303. https://doi.org/10.1029/tc009i006p01275

Carosi, R., Leoni, L., Montomoli, C., & Sartori, F. (2003). Very low-grade metamorphism in the Tuscan Nappe, Northern Apennines, Italy: Relationships between deformation and metamorphic indicators in the La Spezia mega-fold. *Swiss Bulletin of Mineralogy and Petrology*, *83*(1), 15–32.

Carosi, R., Montomoli, C., & Pertusati, P. C. (2004). Late tectonic evolution of the Northern Apennines: The role of contractional tectonics in the exhumation of the Tuscan units. *Geodinamica Acta*, *17*(4), 253–273. https://doi.org/10.3166/ga.17.253-273

Cerrina Feroni, A. G., Plesi, G., Fanelli, G., Leoni, L., & Martinelli, P. (1983). Contributo alla conoscenza dei processi metamorfici di grado molto basso (anchi-metamorfismo) a carico della falda toscana nell'area del ricoprimento apuano. *Bollettino Della Societa Geologica Italiana*, *102*, 269–280.

Chemenda, A. I., Mattauer, M., Malavieille, J., & Bokun, A. N. (1995). A mechanism for syn-collisional rock exhumation and associated normal faulting: Results from physical modeling. *Earth and Planetary Science Letters*, *132*(1–4), 225–232. https://doi.org/10.1016/0012-821x(95)00042-b

Chen, Y.-J., Hjelen, J., & Roven, H. J. (2012). Application of EBSD technique to ultrafine grained and nanostructured materials processed by severe plastic deformation: Sample preparation, parameters optimization and analysis. *Transactions of Nonferrous Metals Society of China*, *22*(8), 1801–1809. https://doi.org/10.1016/s1003-6326(11)61390-3

Chopin, C. (1984). Coesite and pure pyrope in high-grade blueschists of the Western Alps: A first record and some consequences. *Contributions to Mineralogy and Petrology*, *86*(2), 107–118. https://doi.org/10.1007/bf00381838

Chopin, C. (2003). Ultrahigh-pressure metamorphism: Tracing continental crust into the mantle. *Earth and Planetary Science Letters*, *212*(1–2), 1–14. https://doi.org/10.1016/s0012-821x(03)00261-9

Clemenzi, L., Molli, G., Storti, F., Muchez, P., Swennen, R., & Torelli, L. (2014). Extensional deformation structures within a convergent orogen: The Val di Lima low-angle normal fault system (Northern Apennines, Italy). *Journal of Structural Geology*, *66*, 205–222. https://doi.org/10.1016/j.jsg.2014.05.019

Clemenzi, L., Storti, F., Balsamo, F., Molli, G., Ellam, R., Muchez, P., & Swennen, R. (2015). Fluid pressure cycles, variations in permeability, and weakening mechanisms along low-angle normal faults: The Tellaro detachment, Italy. *Geological Society of America Bulletin*, *127*(11–12), 1689–1710. https://doi.org/10.1130/b31203.1

Cloos, M. (1982). Flow melanges: Numerical modeling and geologic constraints on their origin in the Franciscan subduction complex, California. *Geological Society of America Bulletin*, *93*(4), 330–345. https://doi.org/10.1130/0016-7606(1982)93<330:fmnmag>2.0.co;2

Coleman, R. G., & Wang, X. (1995). *Ultrahigh pressure metamorphism*. Cambridge University Press.

Collettini, C., & Holdsworth, R. E. (2004). Fault zone weakening and character of slip along low-angle normal faults: Insights from the Zuccale fault, Elba, Italy. *Journal of the Geological Society*, *161*(6), 1039–1051. https://doi.org/10.1144/0016-764903-179
Conti, P., Cornamusini, G., & Carmignani, L. (2020). An outline of the geology of the Northern Apennines (Italy), with geological map at 1:250,000 scale. *Indian Journal of Gastroenterology*, *139*(2), 149–194. https://doi.org/10.3301/ijg.2019.25
Cowan, D. S., & Silling, R. M. (1978). A dynamic, scaled model of accretion at trenches and its implications for the tectonic evolution of subduction complexes. *Journal of Geophysical Research*, *83*(B11), 5389–5396. https://doi.org/10.1029/jb083ib11p05389
Daniel, J.-M., & Jolivet, L. (1995). Detachment faults and pluton emplacement: Elba Island (Tyrrhenian Sea). *Bulletin de la Societe Geologique de France*, *166*(4), 341–354. https://doi.org/10.2113/gssgfbull.166.4.341
Davis, D., Suppe, J., & Dahlen, F. A. (1983). Mechanics of fold-and-thrust belts and accretionary wedges. *Journal of Geophysical Research*, *88*(B2), 1153–1172. https://doi.org/10.1029/jb088ib02p01153
De Bresser, J. H. P., & Spiers, C. J. (1993). Slip systems in calcite single crystals deformed at 300-800°C. *Journal of Geophysical Research*, *98*(B4), 6397–6409. https://doi.org/10.1029/92jb02044
De Bresser, J. H. P., & Spiers, C. J. (1997). Strength characteristics of the r, f, and c slip systems in calcite. *Tectonophysics*, *272*(1), 1–23. https://doi.org/10.1016/s0040-1951(96)00273-9
Deino, A., Keller, J. V. A., Minelli, G., & Pialli, G. (1992). Datazioni $^{40}Ar/^{39}Ar$ del metamorfismo dell'Unità di Ortano-Rio Marina (Isola d'Elba): Risultati preliminari. *Studi Geologici Camerti*, *2*, 187–192.
Dini, A., Innocenti, F., Rocchi, S., Tonarini, S., & Westerman, D. S. (2002). The magmatic evolution of the late Miocene laccolith-pluton-dyke granitic complex of Elba Island, Italy. *Geological Magazine*, *139*(3), 257–279. https://doi.org/10.1017/s0016756802006556
Duchêne, S., Lardeaux, J. M., & Albarède, F. (1997). Exhumation of eclogites: Insights from depth-time path analysis. *Tectonophysics*, *280*(1–2), 125–140.
Duranti, S., Palmeri, R., Pertusati, P. C., & Ricci, C. A. (1992). Geological evolution and metamorphic petrology of the basal sequences of eastern Elba (complex II). *Acta Vulcanologica*, *2*, 213–229.
Elter, F. M., & Pandeli, E. (2001). Structural evolution of anchi-/epimetamorphic units of Central and Eastern Elba (Ortano, Acquadolce, Monticiano-Roccastrada and Grassera Units). *Ofioliti*, *26*(2a), 219–228.
Elter, P. (1975). Introduction a la geologie de l'Apennin septentrional. *Bulletin de la Societe Geologique de France*, *S7-XVII*(6), 956–962. https://doi.org/10.2113/gssgfbull.s7-xvii.6.956
Elter, P., Giglia, G., Tongiorgi, M., & Trevisan, L. (1975). Tensional and compressional areas in the recent (Tortonian to present) evolution of the Northern Apennines. *Bollettino di Geofisica Teorica e Applicata*, *17*(65), 3–18.
England, P. C., & Holland, T. J. B. (1979). Archimedes and the Tauern eclogites: The role of buoyancy in the preservation of exotic eclogite blocks. *Earth and Planetary Science Letters*, *44*(2), 287–294. https://doi.org/10.1016/0012-821x(79)90177-8
Ernst, W. G. (1970). Tectonic contact between the Franciscan Mélange and the Great Valley Sequence-Crustal expression of a Late Mesozoic Benioff Zone. *Journal of Geophysical Research*, *75*(5), 886–901. https://doi.org/10.1029/jb075i005p00886
Ernst, W. G. (1972). Occurrence and mineralogic evolution of blueschist belts with time. *American Journal of Science*, *272*(7), 657–668. https://doi.org/10.2475/ajs.272.7.657
Ernst, W. G. (2001). Subduction, ultrahigh-pressure metamorphism, and regurgitation of buoyant crustal slices—Implications for arcs and continental growth. *Physics of the Earth and Planetary Interiors*, *127*(1–4), 253–275. https://doi.org/10.1016/s0031-9201(01)00231-x
Ernst, W. G., Maruyama, S., & Wallis, S. (1997). Buoyancy-driven, rapid exhumation of ultrahigh-pressure metamorphosed continental crust. *Proceedings of the National Academy of Sciences of the United States of America*, *94*(18), 9532–9537. https://doi.org/10.1073/pnas.94.18.9532
Escher, A., & Beaumont, C. (1997). Formation, burial and exhumation of basement nappes at crustal scale: A geometric model based on the Western Swiss-Italian Alps. *Journal of Structural Geology*, *19*(7), 955–974. https://doi.org/10.1016/s0191-8141(97)00022-9
Faccenna, C., Becker, T. W., Miller, M. S., Serpelloni, E., & Willett, S. D. (2014). Isostasy, dynamic topography, and the elevation of the Apennines of Italy. *Earth and Planetary Science Letters*, *407*, 163–174. https://doi.org/10.1016/j.epsl.2014.09.027
Faccenna, C., Funiciello, F., Giardini, D., & Lucente, P. (2001). Episodic back-arc extension during restricted mantle convection in the Central Mediterranean. *Earth and Planetary Science Letters*, *187*(1–2), 105–116. https://doi.org/10.1016/s0012-821x(01)00280-1
Fellin, M. G., Reiners, P. W., Brandon, M. T., Wüthrich, E., Balestrieri, M. L., & Molli, G. (2007). Thermochronologic evidence for the exhumational history of the Alpi Apuane metamorphic core complex, northern Apennines, Italy. *Tectonics*, *26*(6). https://doi.org/10.1029/2006tc002085
Ferrill, D. A., Morris, A. P., Evans, M. A., Burkhard, M., Groshong, R. H., Jr, & Onasch, C. M. (2004). Calcite twin morphology: A low-temperature deformation geothermometer. *Journal of Structural Geology*, *26*(8), 1521–1529. https://doi.org/10.1016/j.jsg.2003.11.028
Finetti, I. R., Boccaletti, M., Bonini, M., Del Ben, A., Geletti, R., Pipan, M., & Sani, F. (2001). Crustal section based on CROP seismic data across the North Tyrrhenian–Northern Apennines–Adriatic Sea. *Tectonophysics*, *343*(3–4), 135–163. https://doi.org/10.1016/s0040-1951(01)00141-x
Franceschelli, M., Gianelli, G., Pandeli, E., & Puxeddu, M. (2004). Variscan and Alpine metamorphic events in the northern Apennines (Italy): A review. *Periodico di Mineralogia*, *73*(2), 43–56.
Franceschelli, M., Leoni, L., Memmi, I., & Puxeddu, M. (1986). Regional distribution of Al-silicates and metamorphic zonation in the low-grade Verrucano metasediments from the Northern Apennines, Italy. *Journal of Metamorphic Geology*, *4*(3), 309–321. https://doi.org/10.1111/j.1525-1314.1986.tb00353.x
Gerya, T. V., Stöckhert, B., & Perchuk, A. L. (2002). Exhumation of high-pressure metamorphic rocks in a subduction channel: A numerical simulation. *Tectonics*, *21*(6), 6. https://doi.org/10.1029/2002tc001406
Giorgett, G., Goffé, B., Memmi, I., & Nieto, F. (1998). Metamorphic evolution of Verrucano metasediments in northern Apennines: New petrological constraints. *European Journal of Mineralogy*, *10*(6), 1295–1308. https://doi.org/10.1127/ejm/10/6/1295
Glodny, J., Ring, U., Kühn, A., Gleissner, P., & Franz, G. (2005). Crystallization and very rapid exhumation of the youngest Alpine eclogites (Tauern Window, Eastern Alps) from Rb/Sr mineral assemblage analysis. *Contributions to Mineralogy and Petrology*, *149*(6), 699–712. https://doi.org/10.1007/s00410-005-0676-5
Godin, L., Grujic, D., Law, R. D., & Searle, M. P. (2006). Channel flow, ductile extrusion and exhumation in continental collision zones: An introduction. *Geological Society, London, Special Publications*, *268*(1), 1–23. https://doi.org/10.1144/gsl.sp.2006.268.01.01
Hacker, B. R., Ratschbacher, L., Webb, L., & Shuwen, D. (1995). What brought them up? Exhumation of the Dabie Shan ultrahigh-pressure rocks. *Geology*, *23*(8), 743–746. https://doi.org/10.1130/0091-7613(1995)023<0743:wbtueo>2.3.co;2
Hamilton, W. (1969). Mesozoic California and the underflow of Pacific mantle. *Geological Society of America Bulletin*, *80*(12), 2409–2430. https://doi.org/10.1130/0016-7606(1969)80[2409:mcatuo]2.0.co;2

Jacobs, J., Paoli, G., Rocchi, S., Ksienzyk, A. K., Sirevaag, H., & Elburg, M. A. (2018). Alps to Apennines zircon roller coaster along the Adria microplate margin. *Scientific Reports*, *8*(1), 1–8. https://doi.org/10.1038/s41598-018-20979-w

Jolivet, L., & Brun, J.-P. (2010). Cenozoic geodynamic evolution of the Aegean. *International Journal of Earth Sciences*, *99*(1), 109–138. https://doi.org/10.1007/s00531-008-0366-4

Jolivet, L., Faccenna, C., Goffé, B., Burov, E., & Agard, P. (2003). Subduction tectonics and exhumation of high-pressure metamorphic rocks in the Mediterranean orogens. *American Journal of Science*, *303*(5), 353–409. https://doi.org/10.2475/ajs.303.5.353

Jolivet, L., Faccenna, C., Goffé, B., Mattei, M., Rossetti, F., Brunet, C., et al. (1998). Midcrustal shear zones in postorogenic extension: Example from the northern Tyrrhenian Sea. *Journal of Geophysical Research*, *103*(B6), 12123–12160. https://doi.org/10.1029/97jb03616

Keller, J. V. A., & Coward, M. P. (1996). The structure and evolution of the Northern Tyrrhenian Sea. *Geological Magazine*, *133*(1), 1–16. https://doi.org/10.1017/s0016756800007214

Keller, J. V. A., Minelli, G., & Pialli, G. (1994). Anatomy of late orogenic extension: The Northern Apennines case. *Tectonophysics*, *238*(1–4), 275–294. https://doi.org/10.1016/0040-1951(94)90060-4

Kurz, W., & Froitzheim, N. (2002). The exhumation of eclogite-facies metamorphic rocks—A review of models confronted with examples from the Alps. *International Geology Review*, *44*(8), 702–743. https://doi.org/10.2747/0020-6814.44.8.702

Lamont, T. N., Searle, M. P., Waters, D. J., Roberts, N. M., Palin, R. M., Smye, A., et al. (2019). Compressional origin of the Naxos metamorphic core complex, Greece: Structure, petrography, and thermobarometry. *Bulletin of the Geological Society of America*, *132*(1–2), 149–197. https://doi.org/10.1130/b31978.1

Law, R. D., Searle, M. P., & Godin, L. (2006). *Channel flow, ductile extrusion and exhumation in continental collision zones*. Geological Society of London Special Publication.

Lee, J.-Y., Marti, K., Severinghaus, J. P., Kawamura, K., Yoo, H.-S., Lee, J. B., & Kim, J. S. (2006). A redetermination of the isotopic abundances of atmospheric Ar. *Geochimica et Cosmochimica Acta*, *70*(17), 4507–4512. https://doi.org/10.1016/j.gca.2006.06.1563

Lister, G. S., & Davis, G. A. (1989). The origin of metamorphic core complexes and detachment faults formed during Tertiary continental extension in the northern Colorado River region, U.S.A. *Journal of Structural Geology*, *11*, 65–94. https://doi.org/10.1016/0191-8141(89)90036-9

Lister, G. S., Etheridge, M. A., & Symonds, P. A. (1986). Detachment faulting and the evolution of passive continental margins. *Geology*, *14*(3), 246–250. https://doi.org/10.1130/0091-7613(1986)14<246:dfateo>2.0.co;2

Lo Pò, D., & Braga, R. (2014). Influence of ferric iron on phase equilibria in greenschist facies assemblages: The hematite-rich metasedimentary rocks from the Monti Pisani (Northern Apennines). *Journal of Metamorphic Geology*, *32*(4), 371–387. https://doi.org/10.1111/jmg.12076

Maineri, C., Benvenuti, M., Costagliola, P., Dini, A., Lattanzi, P., Ruggieri, G., & Villa, I. M. (2003). Sericitic alteration at the La Crocetta deposit (Elba Island, Italy): Interplay between magmatism, tectonics and hydrothermal activity. *Mineralium Deposita*, *38*(1), 67–86. https://doi.org/10.1007/s00126-002-0279-2

Mainprice, D., Bachmann, F., Hielscher, R., & Schaeben, H. (2015). Descriptive tools for the analysis of texture projects with large datasets using MTEX: Strength, symmetry and components. *Geological Society, London, Special Publications*, *409*(1), 251–271. https://doi.org/10.1144/sp409.8

Malinverno, A., & Ryan, W. B. F. (1986). Extension in the Tyrrhenian Sea and shortening in the Apennines as result of arc migration driven by sinking of the lithosphere. *Tectonics*, *5*(2), 227–245. https://doi.org/10.1029/tc005i002p00227

Malusà, M. G., Faccenna, C., Baldwin, S. L., Fitzgerald, P. G., Rossetti, F., Balestrieri, M. L., et al. (2015). Contrasting styles of (U)HP rock exhumation along the Cenozoic Adria-Europe plate boundary (Western Alps, Calabria, Corsica). *Geochemistry, Geophysics, Geosystems*, *16*, 1786. https://doi.org/10.1002/2015GC005767

Marroni, M., Meneghini, F., & Pandolfi, L. (2017). A revised subduction inception model to explain the Late Cretaceous, double-vergent orogen in the precollisional Western Tethys: Evidence from the Northern Apennines. *Tectonics*, *36*, 2227–2249. https://doi.org/10.1002/2017TC004627

Maruyama, S., Liou, J. G., & Terabayashi, M. (1996). Blueschists and eclogites of the world and their exhumation. *International Geology Review*, *38*(6), 485–594. https://doi.org/10.1080/00206819709465347

Massa, G., Musumeci, G., Mazzarini, F., & Pieruccioni, D. (2017). Coexistence of contractional and extensional tectonics during the northern Apennines orogeny: The late Miocene out-of-sequence thrust in the Elba Island nappe stack. *Geological Journal*, *52*(3), 353–368. https://doi.org/10.1002/gj.2761

Massonne, H.-J., & Schreyer, W. (1987). Phengite geobarometry based on the limiting assemblage with K-feldspar, phlogopite, and quartz. *Contributions to Mineralogy and Petrology*, *96*(2), 212–224. https://doi.org/10.1007/bf00375235

Massonne, H. J., & Szpurka, Z. (1997). Thermodynamic properties of white micas on the basis of high-pressure experiments in the systems K_2O-MgO-Al_2O_3-SiO_2-H_2O and K_2O-FeO-Al_2O_3-SiO_2-H_2O. *Lithos*, *41*(1–3), 229–250. https://doi.org/10.1016/s0024-4937(97)82014-2

Mauffret, A., Contrucci, I., & Brunet, C. (1999). Structural evolution of the Northern Tyrrhenian Sea from new seismic data. *Marine and Petroleum Geology*, *16*(5), 381–407. https://doi.org/10.1016/s0264-8172(99)00004-5

Mazzarini, F., Musumeci, G., & Cruden, A. R. (2011). Vein development during folding in the upper brittle crust: The case of tourmaline-rich veins of eastern Elba Island, northern Tyrrhenian Sea, Italy. *Journal of Structural Geology*, *33*(10), 1509–1522. https://doi.org/10.1016/j.jsg.2011.07.001

Mazzarini, F., Musumeci, G., Viola, G., Garofalo, P. S., & Mattila, J. (2019). Structural and lithological control on fluid circulation, dilation and ore mineralization (Rio Albano mine, Island of Elba, Italy). *Journal of Structural Geology*, *126*, 210–230. https://doi.org/10.1016/j.jsg.2019.06.012

McDougall, I., & Harrison, T. M. (1999). *Geochronology and thermochronology by the $^{40}Ar/^{39}Ar$ method*. Oxford University Press.

Michard, A., Chopin, C., & Henry, C. (1993). Compression versus extension in the exhumation of the Dora-Maira coesite-bearing unit, Western Alps, Italy. *Tectonophysics*, *221*(2), 173–193. https://doi.org/10.1016/0040-1951(93)90331-d

Miyashiro, A. (1972). Metamorphism and related magmatism in plate tectonics. *American Journal of Science*, *272*(7), 629–656. https://doi.org/10.2475/ajs.272.7.629

Moeller, S., Grevemeyer, I., Ranero, C. R., Berndt, C., Klaeschen, D., Sallarès, V., et al. (2013). Early-stage rifting of the northern Tyrrhenian Sea Basin: Results from a combined wide-angle and multichannel seismic study. *Geochemistry, Geophysics, Geosystems*, *14*(8), 3032–3052. https://doi.org/10.1002/ggge.20180

Moen, K., Malvik, T., Hjelen, J., & Leinum, J. R. (2003). EBSD—A potential supplementary technique in quantitative characterization of minerals. *Paper presented at the XXII International Mineral Processing Congress*. .

Molli, G., Giorgetti, G., & Meccheri, M. (2000). Structural and petrological constraints on the tectono-metamorphic evolution of the Massa Unit (Alpi Apuane, NW Tuscany, Italy). *Geological Journal*, *35*(3-4), 251–264. https://doi.org/10.1002/gj.860

Molli, G., & Malavieille, J. (2011). Orogenic processes and the Corsica/Apennines geodynamic evolution: Insights from Taiwan. *International Journal of Earth Sciences*, *100*(5), 1207–1224. https://doi.org/10.1007/s00531-010-0598-y

Molli, G., Vitale Brovarone, A., Beyssac, O., & Cinquini, I. (2018). RSCM thermometry in the Alpi Apuane (NW Tuscany, Italy): New constraints for the metamorphic and tectonic history of the inner northern Apennines. *Journal of Structural Geology*, *113*, 200–216. https://doi.org/10.1016/j.jsg.2018.05.020

Montomoli, C., Ruggieri, G., Boiron, M. C., & Cathelineau, M. (2001). Pressure fluctuation during uplift of the Northern Apennines (Italy): A fluid inclusions study. *Tectonophysics*, *341*(1–4), 121–139. https://doi.org/10.1016/s0040-1951(01)00197-4

Musumeci, G., Mazzarini, F., & Barsella, M. (2008). Pliocene crustal shortening on the Tyrrhenian side of the northern Apennines: Evidence from the Gavorrano antiform (southern Tuscany, Italy). *Journal of the Geological Society*, *165*(1), 105–114. https://doi.org/10.1144/0016-76492007-004

Musumeci, G., Mazzarini, F., & Cruden, A. R. (2015). The Zuccale Fault, Elba Island, Italy: A new perspective from fault architecture. *Tectonics*, *34*(6), 1195–1218. https://doi.org/10.1002/2014tc003809

Musumeci, G., Mazzarini, F., Tiepolo, M., & Di Vincenzo, G. (2011). U–Pb and 40Ar–39Ar geochronology of Palaeozoic units in the northern Apennines: Determining protolith age and alpine evolution using the Calamita Schist and Ortano Porphyroid. *Geological Journal*, *46*(4), 288–310. https://doi.org/10.1002/gj.1266

Musumeci, G., & Vaselli, L. (2012). Neogene deformation and granite emplacement in the metamorphic units of northern Apennines (Italy): Insights from mylonitic marbles in the Porto Azzurro pluton contact aureole (Elba Island). *Geosphere*, *8*(2), 470–490. https://doi.org/10.1130/ges00665.1

O'Brien, P. J. (2019). Eclogites and other high-pressure rocks in the Himalaya: A review. *Geological Society, London, Special Publications*, *483*, 183–213.

Okay, A. I. (1989). Alpine-Himalayan blueschists. *Annual Review of Earth and Planetary Sciences*, *17*(1), 55–87. https://doi.org/10.1146/annurev.ea.17.050189.000415

Papeschi, S., Musumeci, G., Massonne, H.-J., Bartoli, O., & Cesare, B. (2019). Partial melting and strain localization in metapelites at very low-pressure conditions: The northern Apennines magmatic arc on the Island of Elba, Italy. *Lithos*, *350–351*, 105230. https://doi.org/10.1016/j.lithos.2019.105230

Papeschi, S., Musumeci, G., Massonne, H. J., Mazzarini, F., Ryan, E. J., & Viola, G. (2020). High-P (P = 1.5-1.8 GPa) blueschist from Elba: Implications for underthrusting and exhumation of continental units in the Northern Apennines. *Journal of Metamorphic Geology*, *38*, 495. https://doi.org/10.1111/JMG.12530

Papeschi, S., Musumeci, G., & Mazzarini, F. (2017). Heterogeneous brittle-ductile deformation at shallow crustal levels under high thermal conditions: The case of a synkinematic contact aureole in the inner northern Apennines, southeastern Elba Island, Italy. *Tectonophysics*, *717*, 547–564. https://doi.org/10.1016/j.tecto.2017.08.020

Papeschi, S., Musumeci, G., & Mazzarini, F. (2018). Evolution of shear zones through the brittle-ductile transition: The Calamita Schists (Elba Island, Italy). *Journal of Structural Geology*, *113*, 100–114. https://doi.org/10.1016/j.jsg.2018.05.023

Passchier, C. W., & Rudolph, A. J. T. (2005). *Microtectonics*. Springer Science & Business Media.

Pauselli, C., Barchi, M. R., Federico, C., Magnani, M. B., & Minelli, G. (2006). The crustal structure of the northern Apennines (central Italy): An insight by the CROP03 seismic line. *American Journal of Science*, *306*(6), 428–450. https://doi.org/10.2475/06.2006.02

Pertusati, P. C., Raggi, G., Ricci, C. A., Duranti, S., & Palmeri, R. (1993). Evoluzione post-collisionale dell'Elba centro-orientale. *Memorie Della Societa Geologica Italiana*, *49*, 297–312.

Platt, J. P. (1986). Dynamics of orogenic wedges and the uplift of high-pressure metamorphic rocks. *Geological Society of America Bulletin*, *97*(9), 1037–1053. https://doi.org/10.1130/0016-7606(1986)97<1037:doowat>2.0.co;2

Platt, J. P. (1993). Exhumation of high-pressure rocks: A review of concepts and processes. *Terra Nova*, *5*(2), 119–133. https://doi.org/10.1111/j.1365-3121.1993.tb00237.x

Prior, D. J., Mariani, E., & Wheeler, J. (2009). EBSD in the earth sciences: Applications, common practice, and challenges. In Electron backscatter diffraction in materials science (pp. 345–360). Springer.

Reddy, S. M., Wheeler, J., & Cliff, R. A. (1999). The geometry and timing of orogenic extension: An example from the Western Italian Alps. *Journal of Metamorphic Geology*, *17*, 573–589. https://doi.org/10.1046/j.1525-1314.1999.00220.x

Renne, P. R., Mundil, R., Balco, G., Min, K., & Ludwig, K. R. (2010). Joint determination of ^{40}K decay constants and ^{40}Ar∗/^{40}K for the Fish Canyon sanidine standard, and improved accuracy for ^{40}Ar/^{39}Ar geochronology. *Geochimica et Cosmochimica Acta*, *74*(18), 5349–5367. https://doi.org/10.1016/j.gca.2010.06.017

Ring, U., Brandon, M. T., Willett, S. D., & Lister, G. S. (1999). *Exhumation processes*. Geological Society, London, Special Publications.1

Ring, U., & Glodny, J. (2010). No need for lithospheric extension for exhuming (U)HP rocks by normal faulting. *Journal of the Geological Society*, *167*(2), 225–228. https://doi.org/10.1144/0016-76492009-134

Ring, U., Glodny, J., Will, T., & Thomson, S. (2007). An Oligocene extrusion wedge of blueschist-facies nappes on Evia, Aegean Sea, Greece: Implications for the early exhumation of high-pressure rocks. *Journal of the Geological Society*, *164*(3), 637–652. https://doi.org/10.1144/0016-76492006-041

Ring, U., Glodny, J., Will, T., & Thomson, S. (2010). The Hellenic subduction system: High-pressure metamorphism, exhumation, normal faulting, and large-scale extension. *Annual Review of Earth and Planetary Sciences*, *38*, 45–76. https://doi.org/10.1146/annurev.earth.050708.170910

Ring, U., & Layer, P. W. (2003). High-pressure metamorphism in the Aegean, eastern Mediterranean: Underplating and exhumation from the Late Cretaceous until the Miocene to Recent above the retreating Hellenic subduction zone. *Tectonics*, *22*(3). https://doi.org/10.1029/2001tc001350

Ring, U., Will, T., Glodny, J., Kumerics, C., Gessner, K., Thomson, S., & Drüppel, K. (2007). Early exhumation of high-pressure rocks in extrusion wedges: Cycladic blueschist unit in the eastern Aegean, Greece, and Turkey. *Tectonics*, *26*(2). https://doi.org/10.1029/2005tc001872

Rocchi, S., Westerman, D. S., Dini, A., & Farina, F. (2010). Intrusive sheets and sheeted intrusions at Elba Island, Italy. *Geosphere*, *6*(3), 225–236. https://doi.org/10.1130/ges00551.1

Rogowitz, A., Grasemann, B., Huet, B., & Habler, G. (2014). Strain rate dependent calcite microfabric evolution – An experiment carried out by nature. *Journal of Structural Geology*, *69*, 1–17. https://doi.org/10.1016/j.jsg.2014.08.004

Rosenbaum, G., & Lister, G. S. (2004). Neogene and Quaternary rollback evolution of the Tyrrhenian Sea, the Apennines, and the Sicilian Maghrebides. *Tectonics*, *23*(1). https://doi.org/10.1029/2003tc001518

Rosenbaum, G., Lister, G. S., & Duboz, C. (2002). Reconstruction of the tectonic evolution of the western Mediterranean since the Oligocene. *Journal of the Virtual Explorer*, *8*, 107–130.

Rossetti, F., Faccenna, C., Jolivet, L., Funiciello, R., Goffé, B., Tecce, F., et al. (2001). Structural signature and exhumation P-T-t path of the Gorgona blueschist sequence (Tuscan Archipelago, Italy). *Ofioliti*, *26*(2a), 175–186.
Rossetti, F., Faccenna, C., Jolivet, L., Funiciello, R., Tecce, F., & Brunet, C. (1999). Syn- versus post-orogenic extension: The case study of Giglio Island (Northern Tyrrhenian Sea, Italy). *Tectonophysics*, *304*(1–2), 71–93. https://doi.org/10.1016/s0040-1951(98)00304-7
Rossetti, F., Faccenna, C., Jolivet, L., Goffé, B., & Funiciello, R. (2002). Structural signature and exhumation P-T-t paths of the blueschist units exposed in the interior of the Northern Apennine chain, tectonic implications. *Bollettino Della Societa Geologica Italiana*, *121*(1), 829–842.
Rossetti, F., Tecce, F., Billi, A., & Brilli, M. (2007). Patterns of fluid flow in the contact aureole of the Late Miocene Monte Capanne pluton (Elba Island, Italy): The role of structures and rheology. *Contributions to Mineralogy and Petrology*, *153*(6), 743–760. https://doi.org/10.1007/s00410-006-0175-3
Rubatto, D., & Hermann, J. (2001). Exhumation as fast as subduction? *Geology*, *29*(1), 3–6. https://doi.org/10.1130/0091-7613(2001)029<0003:eafas>2.0.co;2
Schmid, S. M., Panozzo, R., & Bauer, S. (1987). Simple shear experiments on calcite rocks: Rheology and microfabric. *Journal of Structural Geology*, *9*(5–6), 747–778. https://doi.org/10.1016/0191-8141(87)90157-x
Searle, M. P. (2010). Low-angle normal faults in the compressional Himalayan orogen: Evidence from the Annapurna-Dhaulagiri Himalaya, Nepal. *Geosphere*, *6*(4), 296–315. https://doi.org/10.1130/ges00549.1
Searle, M. P., & Lamont, T. N. (2020). Compressional metamorphic core complexes, low-angle normal faults and extensional fabrics in compressional tectonic settings. *Geological Magazine*, *157*(1), 101–118. https://doi.org/10.1017/s0016756819000207
Serri, G., Innocenti, F., & Manetti, P. (1993). Geochemical and petrological evidence of the subduction of delaminated Adriatic continental lithosphere in the genesis of the Neogene-Quaternary magmatism of central Italy. *Tectonophysics*, *223*(1–2), 117–147. https://doi.org/10.1016/0040-1951(93)90161-c
Siivola, J., & Schmid, R. (2007). List of mineral abbreviations. Metamorphic rocks: A classification and glossary of terms. Recommendations of the International Union of Geological Sciences Subcommission on the Systematics of Metamorphic Rocks, 93–110.Cambridge University Press.
Smith, D. C. (1984). Coesite in clinopyroxene in the Caledonides and its implications for geodynamics. *Nature*, *310*(5979), 641–644. https://doi.org/10.1038/310641a0
Sobolev, N. V., & Shatsky, V. S. (1990). Diamond inclusions in garnets from metamorphic rocks: A new environment for diamond formation. *Nature*, *343*(6260), 742–746. https://doi.org/10.1038/343742a0
Sørensen, B. E., Hjelen, J., Ånes, H. W., & Breivik, T. (2020). Recent features in EBSD, including new trapezoidal correction for multi-mapping. *IOP Conference Series: Materials Science and Engineering*, *891*, 012021, 012021. https://doi.org/10.1088/1757-899x/891/1/012021
Storti, F. (1995). Tectonics of the Punta Bianca promontory: Insights for the evolution of the Northern Apennines-Northern Tyrrhenian Sea basin. *Tectonics*, *14*(4), 832–847. https://doi.org/10.1029/95tc01203
Theye, T., Reinhardt, J., Goffé, B., Jolivet, L., & Brunet, C. (1997). Ferro- and magnesiocarpholite from the Monte Argentario (Italy): First evidence for high-pressure metamorphism of the metasedimentary Verrucano sequence, and significance for P-T path reconstruction. *European Journal of Mineralogy*, *9*, 859–874. https://doi.org/10.1127/ejm/9/4/0859
Thomson, S. N., Stöckhert, B., & Brix, M. R. (1999). Miocene high-pressure metamorphic rocks of Crete, Greece: Rapid exhumation by buoyant escape. *Geological Society, London, Special Publications*, *154*(1), 87–107. https://doi.org/10.1144/gsl.sp.1999.154.01.04
Trevisan, L. (1950). *L'Elba orientale e la sua tettonica di scivolamento per gravità*. Società Cooperativa Tipografica.
Trullenque, G., Kunze, K., Heilbronner, R., Stünitz, H., & Schmid, S. M. (2006). Microfabrics of calcite ultramylonites as records of coaxial and non-coaxial deformation kinematics: Examples from the Rocher de l'Yret shear zone (Western Alps). *Tectonophysics*, *424*(1–2), 69–97. https://doi.org/10.1016/j.tecto.2006.06.004
Tsujimori, T., & Ernst, W. G. (2014). Lawsonite blueschists and lawsonite eclogites as proxies for palaeo-subduction zone processes: A review. *Journal of Metamorphic Geology*, *32*(5), 437–454. https://doi.org/10.1111/jmg.12057
Vai, G. B., & MartiniI. P. (Eds.), (2001). *Anatomy of an orogen: The Apennines and adjacent Mediterranean basins*. Kluwer Academic Publishers.
Van Hinsbergen, D. J. J., Zachariasse, W. J., Wortel, M. J. R., & Meulenkamp, J. E. (2005). Underthrusting and exhumation: A comparison between the External Hellenides and the "hot" Cycladic and "cold" South Aegean core complexes (Greece). *Tectonics*, *24*(2). https://doi.org/10.1029/2004tc001692
Vidal, O., & Parra, T. (2000). Exhumation paths of high-pressure metapelites obtained from local equilibria for chlorite-phengite assemblages. *Geological Journal*, *35*(3–4), 139–161. https://doi.org/10.1002/gj.856
Vignaroli, G., Faccenna, C., Jolivet, L., Piromallo, C., & Rossetti, F. (2008). Subduction polarity reversal at the junction between the Western Alps and the Northern Apennines, Italy. *Tectonophysics*, *450*, 34–50. https://doi.org/10.1016/j.tecto.2007.12.012
Vignaroli, G., Faccenna, C., Rossetti, F., & Jolivet, L. (2009). Insights from the Apennines metamorphic complexes and their bearing on the kinematics evolution of the orogen. *Geological Society, London, Special Publications*, *311*(1), 235–256. https://doi.org/10.1144/sp311.9
Viola, G. (2021). *"Ryan et al., 2021", Mendeley Data, V2*, http://dx.doi.org/10.17632/bj3nwk3wpm.2
Viola, G., Torgersen, E., Mazzarini, F., Musumeci, G., Lelij, R., Schönenberger, J., & Garofalo, P. S. (2018). New constraints on the evolution of the inner Northern Apennines by K-Ar dating of Late Miocene-Early Pliocene compression on the Island of Elba, Italy. *Tectonics*, *37*(9), 3229–3243. https://doi.org/10.1029/2018tc005182
Warren, C. J. (2013). Exhumation of (ultra-)high-pressure terranes: Concepts and mechanisms. *Solid Earth*, *4*, 75–92. https://doi.org/10.5194/se-4-75-2013
Wenk, H. R., Takeshita, T., Van Houtte, P., & Wagner, F. (1986). Plastic anisotropy and texture development in calcite polycrystals. *Journal of Geophysical Research*, *91*(B3), 3861–3869. https://doi.org/10.1029/jb091ib03p03861
Westerman, D. S., Dini, A., Innocenti, F., & Rocchi, S. (2004).Rise and fall of a nested Christmas-tree laccolith complex, Elba Island, Italy, *Geological Society, London, Special Publications*, *234*(1), 195–213. https://doi.org/10.1144/gsl.sp.2004.234.01.12
Wheeler, J., Reddy, S. M., & Cliff, R. A. (2001). Kinematic linkage between internal zone extension and shortening in more external units in the NW Alps. *Journal of the Geological Society*, *158*(3), 439–443. https://doi.org/10.1144/jgs.158.3.439
Whitney, D. L., Teyssier, C., Rey, P., & Buck, W. R. (2013). Continental and oceanic core complexes. *The Geological Society of America Bulletin*, *125*(3–4), 273–298. https://doi.org/10.1130/b30754.1